Available online at www.sciencedirect.com
ScienceDirect
Lithos 96 (2007) 475–502
LITHOS
www.elsevier.com/locate/lithos

Geochronological, geochemical and geothermal constraints on petrogenesis of the Indosinian peraluminous granites in the South China Block: A case study in the Hunan Province

Yuejun Wang [a,b,*], Weiming Fan [a], Min Sun [b], Xinquan Liang [a], Yanhua Zhang [c], Touping Peng [a]

[a] *Key Laboratory of Isotope Geochronology and Geochemistry, Guangzhou Institute of Geochemistry, Chinese Academy of Sciences, Guangzhou 510640, China*
[b] *Department of Earth Sciences, The University of Hong Kong, Pokfulam Road, Hong Kong*
[c] *CSIRO Exploration and Mining, PO Box 1130, Bentley, WA 6102, Australia*

Received 17 April 2006; accepted 15 November 2006
Available online 9 January 2007

Abstract

The Indosinian granites in the South China Block (SCB) have important tectonic significance for the evolution of East Asia. Samples collected from Hunan Province can be geochemically classified into two groups. Group 1 is strongly peraluminous (A/CNK > 1.1), similar to S-type granites, and Group 2 has A/CNK = 1.0–1.1, with an affinity to I-type granites. Group 1 has lower FeOt, Al_2O_3, MgO, CaO, TiO_2 and $\varepsilon_{Nd}(t)$ values but higher K_2O+Na_2O, Rb/Sr, Rb/Ba and $^{87}Sr/^{86}Sr(t)$ than those of Group 2. Samples of both groups have similar LREE enriched pattern, with (Eu/Eu*) = 0.19–0.69, and strongly negative Ba, Sr, Nb, P and Ti anomalies. Geothermobarometry study indicates that the precursor magmas were emplaced at high-level depth with relatively low temperature (734–827 °C). Geochemical data suggest that Group 1 was originated from a source dominated by pelitic composition and Group 2 was from a mixing source of pelitic and basaltic rocks with insignificant addition of newly mantle-derived magma. Eight granitic samples in Hunan Province are dated at the cluster of 243–235 and 218–210 Ma by zircon U–Pb geochronology. Together with recent zircon U–Pb ages for other areas in the SCB, two age-clusters, including 243–228 Ma just after peak-metamorphism (~246–252 Ma) and 220–206 Ma shortly after magma underplating event (~224 Ma), are observed. It is proposed that in-situ radiogenic heating from the over-thickened crust induced dehydrated reaction of muscovite and epidote/zoisite to form the early Indosinian granites in response to the isostatic readjustments of tectonically thickened crust. Conductive heating from the underplating magma in the postcollisional setting triggered the formation of late Indosinian granites. Such a consideration is supported by the results from FLAC numerical simulation.

Keywords: Geochemistry; Zircon U–Pb geochronology; Indosinian granites; Tectonically crustal thickening; South China Block

1. Introduction

South China Block (SCB) is composed of the Yangtze and outboard Cathaysian tectonic regions (or Yangtze and Cathaysian blocks). Indosinian granites

* Corresponding author. Current address: Guangzhou Institute of Geochemistry, Chinese Academy of Sciences, P.O. Box 1131, Guangzhou 510640, People's Republic of China. Tel.: +86 20 85290527; fax: +86 20 85291510.
E-mail address: yjwang@gig.ac.cn (Y. Wang).

0024-4937/$ - see front matter © 2006 Elsevier B.V. All rights reserved.
doi:10.1016/j.lithos.2006.11.010

within the SCB have attracted considerable attentions since the "Indosinian movement", which was also named Indosinian Orogeny originally recorded by unconformities between pre-Norian and pre-Rhaetian during Triassic in Vietnam (Deprat, 1914; Fromagat, 1932), was proposed (e.g., JXGBMR, 1984; Huang et al., 1987; HNGBMR, 1988; Ren, 1991; Chen and Jahn, 1998; Shen et al., 1998; Wang et al., 2002, 2003a,b,c; Deng et al., 2004; Qiu et al., 2004, 2005a,b,c). Previous studies showed that these granites are of large volume and mainly distributed in the central SCB (particularly in Hunan and Guangxi Provinces), far away from the continental margins (e.g., Huang et al., 1987; Chen and Jahn, 1998), and occur as laccoliths and batholiths along fault zones or fault intersections (JXGBMR, 1984; HNGBMR, 1988). These rocks were traditionally grouped as the Hercynian–Indosinian peraluminous S-type granites, and their high initial Sr isotopic ratios have been realized (Shen et al., 1998; Chen and Jahn, 1998).

However, due to the lack of precisely geochronological and systematically geochemical data, their petrogenesis remains poorly constrained and the tectonic implications have long been debated. Two controversial hypotheses have been proposed for the magma generation, including (i) the anatexis of thickened crust in the compressive setting due to the collision between the Yangtze and Cathaysian blocks probably along the Chenzhou–Linwu fault (e.g., Wang et al., 2003b, 2005b), and (ii) derivation of the newly underplating magma in response to upwelling asthenosphere.

The Indosinian granites were collected from Hunan Province for this study, where is the type region with predominant outcrops of the Indosinian granites in the SCB (e.g., Huang et al., 1987; HNGBMR, 1988; Wang et al., 2002, 2005a). Geochronological, elemental and Sr–Nd isotopic studies for these granites were conducted in order to better understand the petrogenesis and the implications on the Indosinian tectonic evolution of the SCB.

2. Geological setting, field relationships and petrography

The Yangtze and Cathaysian blocks in the SCB have distinctive crustal ages and tectonic histories (Huang et al., 1987; HNGBMR, 1988; Ren, 1991; JXGBMR, 1984). The basement of the Yangtze block consists of Archean rocks up to >3.2 Ga, with an average age of 2.7–2.8 Ga (Gao et al., 1999; Qiu et al., 2000). The basement of the Cathaysian block is dominantly Paleo- to Mesoproterozoic, with some late Achaean component (~2.5 Ga; JXGBMR, 1989; Chen and Jahn, 1998). It is generally considered that the two blocks were amalgamated during the Jinningian (or Grenvillian) orogeny (e.g., Li et al., 2002). Subsequently, a failed rifting was developed roughly along the suture during the Neoproterozic and Paleozoic, geographically through Hunan, Jiangxi, western Guangdong and eastern Guangxi Provinces. The failed rifting was manifested by the >13 km thick deposition of Neoproterozoic–Paleozoic abyssal marine carbonatitic/clastic sequence in the center and the 2–5 km shallow-sea carbonate deposits limited to the rifting margins (e.g., JXGBMR, 1984; HNGBMR, 1988; Wang and Li, 2003). These pre-Mesozoic sequences are overprinted by the Indosinian tectonothermal event and unconformably overlain by the lower Mesozoic terrestrial clastics (JXGBMR, 1984; HNGBMR, 1988). The Indosinian mafic magmatism is missing except for some gabbroic xenoliths (~224 Ma) hosted by Mesozoic basalts in Daoxian, southern Hunan Province (Guo et al., 1997).

The Indosinian granitic plutons predominantly outcrop in the failed rifting zone bounded by the Anhua–Luocheng and Heyuan–Guangfeng faults, geographically in the region between Xuefeng Mountains and Wuyi–Baiyun–Yunkai Mountains (Fig. 1a). These granites intruded the pre-Triassic strata as stocks and batholiths (JXGBMR, 1984; HNGBMR, 1988), and are mainly coarse- to medium-grained peraluminous granites and granodiorites with massive textures. The strongly peraluminous plutons in the Yunkai Mountains are dominantly muscovite-, garnet- and tourmaline-bearing leucogranites with gneissic texture, and cordierite is common but enclaves are rarely found (e.g., Deng et al., 2004). In contrast, the weakly peraluminous granites and granodiorites contain abundant angular to rounded enclaves, and hornblende is occasionally observed. Contacts with the country rocks are commonly sharp, but contact metamorphism is not prominent.

Hunan Province is the type region for distribution of the Indosinian granites in the SCB, where these plutons occupy areas of >5600 km^2 (HNGBMR, 1988). Previously geochronological studies (e.g., whole-rocks Rb–Sr, K–Ar and grain-zircon U–Pb methods) gave age-span of 163–267 Ma, mostly between 185 Ma and 235 Ma (HNGBMR, 1988). These granites in Hunan mainly outcropped in the region between the Chenzhou–Linwu and Anhua–Luocheng faults, and intruded the pre-Triassic sequences as stocks and batholiths (HNGBMR, 1988). The main plutons include Taojiang, Xiangzikou, Tangshi, Dingziwan, Dashenshan, Baimashan, Ziyunshan, Xiema, Tashan, Guandimiao, Wawutang,

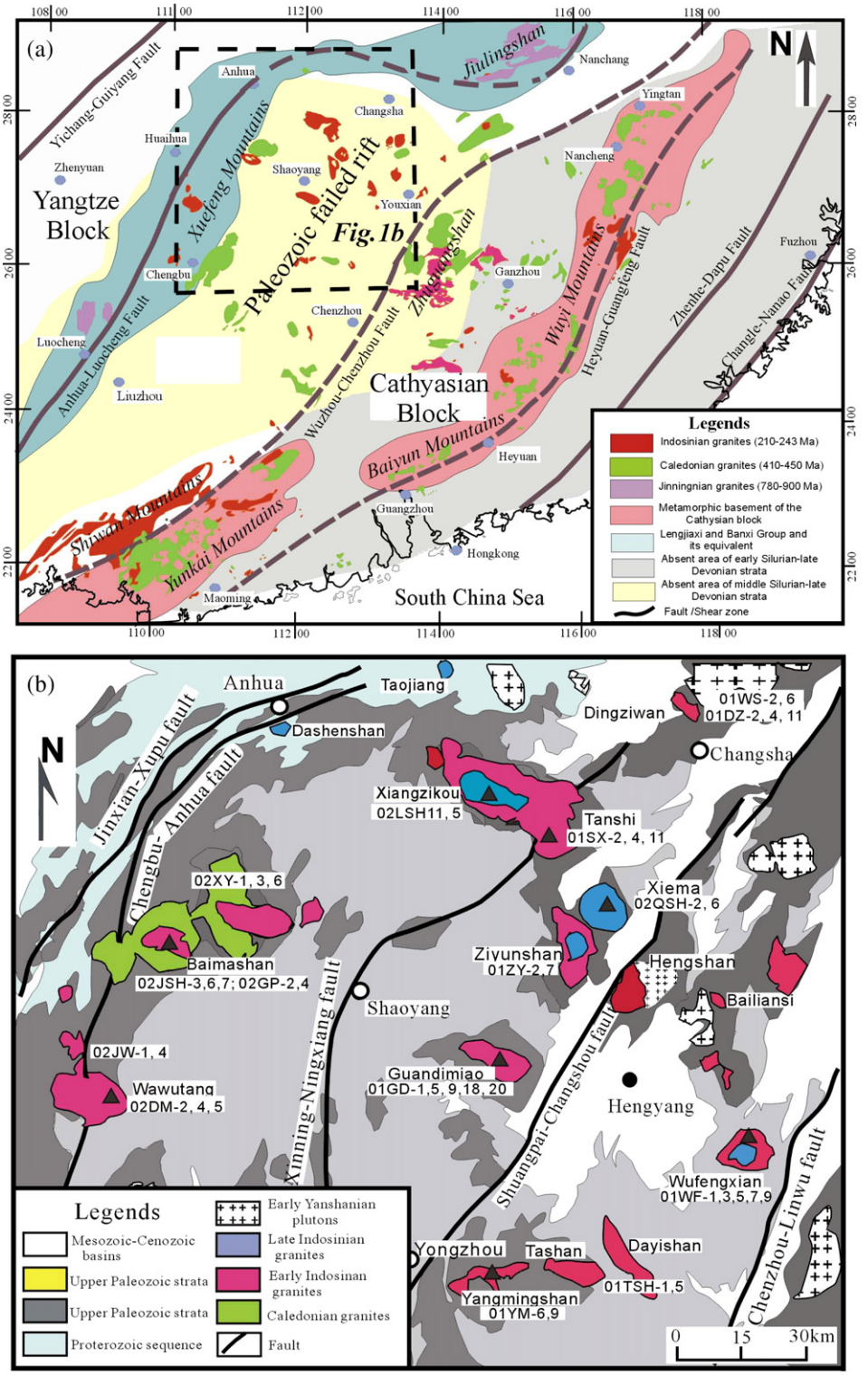

Fig. 1. (a) Simplified geological map of the South China Block showing the distribution of the Indosinian granitic plutons (JXGBMR, 1984; HNGBMR, 1988); (b) Geological map showing the Indosinian granitic plutons in Hunan Province, revised from the 1:1,000,000 geological map of Hunan Provinces (HNGBMR, 1988). The symbols of triangles refer to sampling locations for zircon U–Pb analyses.

Yangmingshan, Dayishan, Jiangjunmiao and Wufengxian intrusions (Fig. 1b). They are dominantly two-mica monzonitic granites, biotite monzonitic granite and muscovite-(garnet) granites with insignificant deformation. The biotite granodiorites and hornblende granite are rare.

The most common mineral assemblage of these granites in Hunan Province is biotite–plagioclase–K-feldspar–quartz with minor amount of muscovite and accessory minerals (e.g., tourmaline, apatite, zircon, monazite and Fe–Ti oxides), and proportions of alkali feldspar to plagioclase are variable. They are coarse- to mediated-grained (1–5 mm), and show porphyritic textures with feldspar phenocrysts mostly from 3 to 8 mm, occasionally up to 30 mm long, and the matrix is mainly composed of fine-grained K-feldspar, plagioclase, quartz and minor biotite. Plagioclase occurs as euhedral to subhedral crystals with An=15–45, some with Carlsbad twins. K-feldspar, mainly perthitic microcline, contains euhedral inclusions of plagioclase and round quartz grains. Quartz occurs as up to 10 mm grain, and biotite occurs either as mineral aggregates or as individual crystals, and usually contains small inclusion of haloed zircon and euhedral apatite. Garnet and amphibole are rarely observed in the investigated samples. Deformation characterized by the undulatory extinction of quartz, kinking and fracture structures of plagioclase and bending of biotite is observed for the some plutons (Xu et al., 2003; Wang et al., 2005a).

3. Analytical methods

All samples were crushed to 200-mesh using an agate mill for major, trace element and Sr–Nd isotopic analyses. Major elements were determined by X-ray fluorescence spectrometry at the Hubei Institute of Geology and Mineral Resource, the Chinese Ministry of Land and Resources. FeO content is analyzed by wet chemical method. The samples were analyzed for trace element contents using inductively coupled plasma-mass spectrometer (ICP-MS) at the Institute of Geochemistry, the Chinese Academy of Sciences (CAS). Detailed sample preparation and analytical procedure followed Qi et al. (2000).

Sr and Nd isotopic ratios were measured by MC-ICP-MS at the Guangzhou Institute of Geochemistry, CAS. Sample preparation and chemical separation followed Liang et al. (2003). The total procedure blanks were in the range of 200–500 pg for Sr and ≤50 pg for Nd. The mass fractionation corrections for Sr and Nd isotopic ratios are based on $^{86}Sr/^{88}Sr=0.1194$ and $^{146}Nd/^{144}Nd=0.7219$, respectively. The measured $^{87}Sr/^{86}Sr$ ratio of the (NIST) SRM 987 standard and $^{143}Nd/^{144}Nd$ ratio of the La Jolla standard is 0.710265 ± 12 (2σ) and 0.511862 ± 10 (2σ), respectively.

Zircons were separated by conventional heavy liquid and magnetic techniques. The separates were mounted in epoxy, polished and coated with gold. The mounts were then photographed in transmitted and reflected light, and the cathodoluminescence (CL) image technique was used to examine the internal structure of analyzed zircons.

The U–Pb isotopic determination was undertaken on the polished mount using a sensitive high-resolution ion microprobe (SHRIMP II) at the Beijing SHRIMP Center, Chinese Academy of Geological Sciences. Detailed analytical procedures of SHRIMP are similar to those described by Compston et al. (1992) and Williams (1998). The standard TEM zircons (age of 417 Ma) of RSES were used to determine the elemental discrimination that occurs during sputter ionization. The calculation of $^{206}Pb/^{238}U$ ages is based on the assumption that the bias in the measured $^{206}Pb/^{238}U^{+}$ ratio can be described by the same power law relationship between $^{206}Pb/^{238}U^{+}$ and UO^{+}/U^{+} for both the zircon standard and sample. Common Pb correction was made using the observed ^{204}Pb peak. Data processing was carried out using the Isoplot programs of Ludwig (2001).

Laser ablation ICPMS (LA-ICPMS) zircon U–Pb analyses were carried out at the laboratory of Northwest University in Xi'an, China, using an Elan 6100 DRC ICP-MS from Perkin Elmer/SCIEX. The GeoLas 200M laser ablation system (MicroLas, Göttingen, Germany) was used for laser ablation. The measurements were carried out using time resolved analysis operating in a fast, peak-hopping sequence in the DUAL detector mode. $^{207}Pb/^{206}Pb$ and $^{206}Pb/^{238}U$ ratios were calculated using GLITTER 4.0 (Jackson et al., 2004). Detailed analytical procedures are similar to those described by Yuan et al. (2003). The zircon standard TEMORA1 yielded a weighted $^{206}Pb/^{238}U$ age of 415 ± 4 Ma (MSWD=0.11; Yuan et al., 2003), which is in agreement with the recommended ID-TIMS age of 416.7 ± 0.2 Ma.

4. Geochemical results

Geochemical data for the samples of the Indosinian granites collected from Hunan Province are presented in Table 1. The samples from the Wufengxian, Tashan, Yangmingshan, Ziyunshan, Dingziwan and Wushi plutons are strongly peraluminous, with A/CNK (molar $Al_2O_3/CaO+Na_2O+K_2O$)>1.1 (Fig. 2a) and

Table 1
Major and trace element analyses for the Indosinian peraluminous granites in Hunan Province

Samples	Group 1													
	Wufengxian					Tashan		Yangmingshan		Ziyunshan		Dingziwan		
	01WF01	01WF03	01WF05	01WF07	01WF09	02TSH01	02TSH5	01YM06	01YM09	01ZY02	01ZY07	01DZ02	01DZ04	01DZ11
SiO_2	75.38	75.72	75.50	75.32	75.17	73.34	73.71	74.30	76.49	74.19	74.13	74.51	74.31	73.39
Al_2O_3	13.56	13.33	13.61	13.50	13.70	13.88	13.70	13.18	12.89	13.67	13.44	14.14	14.25	14.43
Fe_2O_3	0.04	0.08	0.10	0.04	0.05	0.11	0.14	0.34	0.38	0.05	0.01	0.08	0.02	0.05
FeO	0.95	0.82	0.97	0.85	0.65	1.55	1.60	1.27	0.60	1.40	1.65	0.85	0.92	1.20
MgO	0.35	0.41	0.34	0.36	0.33	0.70	0.72	0.57	0.29	0.46	0.58	0.34	0.34	0.55
CaO	0.89	0.72	0.78	0.82	0.85	1.82	1.45	0.87	0.45	1.20	1.35	1.13	1.20	1.84
Na_2O	3.32	3.39	3.32	3.13	3.31	2.77	2.94	3.00	3.94	2.59	2.88	3.45	3.62	3.20
K_2O	4.05	3.90	4.10	4.55	4.70	4.38	4.38	4.46	3.74	5.08	4.55	4.17	4.14	4.04
MnO	0.05	0.04	0.04	0.04	0.03	0.03	0.04	0.05	0.05	0.03	0.04	0.04	0.04	0.02
TiO_2	0.13	0.14	0.11	0.10	0.09	0.24	0.24	0.25	0.13	0.19	0.22	0.11	0.12	0.25
P_2O_5	0.16	0.18	0.17	0.16	0.16	0.09	0.08	0.20	0.20	0.10	0.09	0.13	0.15	0.11
LOI	0.97	1.00	0.91	0.98	0.82	1.09	0.99	1.39	0.78	0.88	0.90	0.89	0.72	0.73
Total	99.85	99.73	99.95	99.85	99.86	100.0	99.99	99.88	99.89	99.84	99.84	99.84	99.83	99.81
A/NK	1.38	1.36	1.37	1.34	1.30	1.49	1.43	1.35	1.22	1.40	1.39	1.39	1.36	1.50
A/CNK	1.18	1.20	1.20	1.17	1.13	1.10	1.12	1.16	1.13	1.14	1.11	1.15	1.13	1.11
Sc		2.70	2.85	2.30	2.29	4.82	5.26	3.75	4.35	3.90	4.67		3.12	3.40
V		6.49	6.99	5.88	5.16	15.16	18.86	13.23	13.43	11.72	13.83		6.73	13.41
Cr		6.64	6.41	4.83	7.97	11.85	15.01	8.35	13.74	10.34	9.32		3.78	6.15
Co		1.17	1.18	1.07	0.91	2.93	3.37	2.38	2.58	2.08	2.54		1.26	2.27
Ni		2.98	2.83	3.24	3.73	5.96	7.15	4.37	11.64	6.02	18.88		3.04	3.19
Ga		18.6	17.6	17.0	15.8	21.0	20.2	21.0	18.3	17.9	18.3		18.5	20.0
Rb		305	318	274	264	357	341	317	234	324	301		305	245
Sr		51.2	56.4	61.3	58.8	43.4	45.6	43.8	39.5	76.1	70.4		115.2	186.8
Y		10.54	11.05	11.04	9.59	15.27	16.23	13.02	13.07	17.69	15.03		9.31	5.58
Zr		58.8	66.4	65.4	63.5	111.5	108.6	115.6	94.0	107.1	116.1		65.3	116.1
Nb		15.43	14.79	12.41	11.13	14.03	13.45	14.42	16.59	13.71	16.32		9.47	6.99
Cs		38.14	39.62	42.02	41.06	53.18	69.84	19.19	12.38	24.74	29.82		48.35	39.70
Ba		126	144	196	191	184	261	182	171	319	259		263	495
La		21.10	22.26	21.19	19.89	24.99	24.59	28.41	15.86	32.63	38.84		16.05	31.32
Ce		40.70	43.04	42.64	39.56	53.41	50.08	61.56	54.05	63.06	74.62		28.58	54.15
Pr		4.79	5.00	4.78	4.45	6.48	6.10	7.64	4.10	7.16	8.32		2.94	5.60
Nd		16.38	17.59	16.16	15.70	24.10	22.31	27.66	14.99	24.12	28.29		9.75	18.47
Sm		3.26	3.36	3.26	3.11	4.95	4.80	5.22	3.33	4.84	5.45		2.11	3.22
Eu		0.34	0.35	0.36	0.37	0.40	0.48	0.31	0.21	0.49	0.46		0.32	0.57
Gd		2.77	2.84	2.74	2.45	4.05	3.99	4.22	2.82	4.15	4.64		2.00	2.32
Tb		0.41	0.39	0.40	0.36	0.59	0.59	0.56	0.45	0.62	0.62		0.30	0.26
Dy		1.90	1.98	2.04	1.79	3.13	3.03	2.62	2.47	3.30	3.09		1.68	1.16
Ho		0.33	0.37	0.35	0.32	0.59	0.60	0.47	0.50	0.62	0.52		0.29	0.17

(continued on next page)

Table 1 (*continued*)

Samples	Group 1													
	Wufengxian					Tashan		Yangmingshan		Ziyunshan		Dingziwan		
	01WF01	01WF03	01WF05	01WF07	01WF09	02TSH01	02TSH5	01YM06	01YM09	01ZY02	01ZY07	01DZ02	01DZ04	01DZ11
Er		0.86	0.93	0.94	0.81	1.63	1.63	1.16	1.19	1.64	1.40		0.74	0.47
Tm		0.14	0.14	0.15	0.13	0.23	0.25	0.15	0.17	0.23	0.19		0.11	0.05
Yb		0.79	0.89	0.90	0.76	1.52	1.58	1.01	1.20	1.36	1.30		0.60	0.38
Lu		0.12	0.13	0.14	0.11	0.23	0.25	0.14	0.18	0.21	0.18		0.09	0.05
Hf		2.10	2.32	2.21	2.12	3.46	3.15	3.51	3.03	3.47	3.71		2.14	3.30
Ta		3.12	3.21	2.68	2.35	3.11	2.99	2.84	3.23	2.05	2.61		2.43	1.25
Pb		34.9	37.9	41.8	82.4	36.1	35.6	30.3	30.2	51.3	52.5		48.5	96.6
Th		16.2	17.7	18.1	15.6	21.4	16.9	27.0	23.3	27.9	32.5		9.5	18.8
U		6.58	6.57	5.94	3.87	9.05	6.07	11.17	6.92	4.17	4.35		3.69	4.42

Samples	Group 1		Group 2											
	Wushi		Baimashan								Congyangping		Xiangzikou	
	01WS02	01WS06	02JSH3	02JSH6	02JSH7	02GP04	02GP06	02XY01	02XY03	02XY06	02JW01	02JW04	02LSH1	02LSH5
SiO_2	73.61	73.58	69.96	69.41	69.95	70.02	70.05	69.65	71.55	69.68	69.97	70.48	71.80	71.79
Al_2O_3	14.30	14.29	14.36	14.27	14.77	14.53	14.85	14.86	14.07	14.99	14.45	14.23	14.44	14.30
Fe_2O_3	0.05	0.07	0.28	0.38	0.30	0.32	0.28	0.21	0.21	0.13	0.04	0.16	0.24	0.24
FeO	1.30	1.18	2.33	2.57	2.33	2.38	2.30	2.32	1.98	2.30	2.80	2.67	1.70	1.83
MgO	0.51	0.55	1.56	2.30	1.60	1.54	1.33	1.40	1.21	1.37	1.24	1.19	0.86	0.86
CaO	1.53	1.61	2.92	3.23	2.96	3.08	3.25	2.96	2.50	2.91	2.31	2.31	2.00	2.00
Na_2O	3.28	3.28	2.82	2.23	2.78	2.93	3.19	3.23	2.95	3.22	2.72	2.80	2.97	2.96
K_2O	4.19	4.20	3.14	3.24	3.77	3.52	3.08	3.62	3.95	3.71	4.37	4.30	4.52	4.50
MnO	0.03	0.04	0.05	0.14	0.05	0.05	0.05	0.05	0.05	0.05	0.06	0.06	0.04	0.04
TiO_2	0.21	0.21	0.39	0.83	0.40	0.41	0.35	0.38	0.32	0.36	0.48	0.50	0.28	0.29
P_2O_5	0.10	0.10	0.12	0.17	0.11	0.11	0.13	0.10	0.09	0.10	0.16	0.16	0.12	0.12
LOI	0.74	0.71	0.88	1.20	0.80	0.92	0.95	1.04	0.96	0.99	1.23	0.97	0.87	0.94
Total	99.85	99.82	98.81	99.97	99.82	99.81	99.81	99.82	99.84	99.81	99.83	99.83	99.84	99.87
A/NK	1.44	1.44	1.78	1.99	1.70	1.68	1.73	1.61	1.54	1.61	1.57	1.53	1.47	1.47
A/CNK	1.12	1.11	1.07	1.09	1.05	1.02	1.02	1.02	1.03	1.03	1.08	1.06	1.07	1.07
Sc	3.72	3.79	6.66	22.61		7.25	7.07		6.95	7.50	6.11	6.33	5.78	5.55
V	14.18	13.74	41.66	111.6		43.39	35.92		37.46	41.11	41.48	41.77	22.80	25.17
Cr	12.78	12.89	41.23	100.8		41.02	34.28		30.19	34.16	19.14	20.56	15.89	17.61
Co	2.28	2.34	8.32	20.91		8.12	6.82		6.15	7.21	7.26	6.66	4.25	4.54
Ni	6.30	18.18	22.64	52.19		26.26	19.47		14.97	18.34	9.53	10.93	7.17	8.26
Ga	21.1	21.5	17.7	21.9		17.8	18.4		16.7	17.7	17.6	17.7	17.4	18.6
Rb	271	268	231	248		202	191		210	206	175	188	258	264
Sr	143	149	142	109		138	135		140	169	96.3	101	103	103
Y	7.86	7.51	13.67	31.46		12.48	11.17		14.45	13.95	14.04	15.04	12.84	14.04
Zr	102	102	160	206		152	188		157	155	187	183	135	144

Nb	8.09	7.94	9.36	15.94	9.36	10.21	8.40	9.43	13.32	13.49	10.97	11.85
Cs	34.73	34.00	22.84	32.78	24.10	25.98	17.16	17.74	17.53	19.35	30.51	30.78
Ba	344	346	481	701	409	380	475	576	417	479	369	379
La	32.52	31.91	34.36	25.10	27.74	24.93	43.55	38.43	23.18	25.25	37.43	41.33
Ce	55.86	55.53	65.11	51.95	50.63	56.92	77.98	69.25	46.04	51.93	71.38	80.49
Pr	5.92	5.82	7.17	6.47	5.59	5.37	8.26	7.31	5.62	6.15	7.88	8.84
Nd	19.10	18.64	24.54	25.57	19.23	18.33	27.52	25.39	19.94	21.27	27.89	31.62
Sm	3.01	2.89	4.14	6.54	3.53	3.65	4.52	4.01	4.17	4.34	5.51	5.94
Eu	0.50	0.47	0.77	0.71	0.79	0.70	0.66	0.84	0.65	0.67	0.68	0.66
Gd	2.28	2.24	3.60	6.72	3.08	3.15	3.66	3.66	3.66	3.88	4.67	5.09
Tb	0.31	0.30	0.48	1.03	0.44	0.42	0.51	0.48	0.51	0.55	0.55	0.61
Dy	1.45	1.43	2.45	6.20	2.23	2.18	2.69	2.57	2.87	3.07	2.65	2.86
Ho	0.27	0.26	0.51	1.25	0.46	0.41	0.54	0.53	0.57	0.59	0.51	0.49
Er	0.71	0.64	1.40	3.16	1.20	1.17	1.50	1.43	1.51	1.61	1.31	1.49
Tm	0.09	0.09	0.20	0.47	0.19	0.17	0.21	0.21	0.22	0.22	0.20	0.22
Yb	0.62	0.57	1.23	2.70	1.16	1.06	1.44	1.40	1.40	1.47	1.17	1.29
Lu	0.07	0.09	0.18	0.38	0.17	0.16	0.23	0.22	0.20	0.22	0.19	0.19
Hf	3.03	3.19	4.42	5.42	4.07	5.15	4.32	4.22	5.17	5.07	3.92	4.29
Ta	1.63	1.75	1.29	1.22	1.26	1.20	0.91	1.00	1.40	1.42	1.59	1.74
Pb	39.4	112.0	45.9	27.5	38.4	39.6	56.4	49.7	30.7	30.9	47.5	73.2
Th	18.8	18.9	24.3	18.5	18.2	27.1	24.2	27.4	17.6	18.7	26.2	30.0
U	7.24	5.63	4.08	3.60	4.31	5.66	6.82	6.01	6.90	4.83	9.13	8.55

Samples	Group 2												
	Guangdimiao					Xiema			Tangshi		Wawutang		
	01GD01	01GD05	01GD09	01GD18	01GD20	01XM01	01XM04	01XM12	02QSH2	02QSH6	02DM2	02DM4	02DM5
SiO_2	71.59	70.81	71.81	71.51	70.70	68.25	68.34	68.73	70.64	70.61	70.78	71.74	72.04
Al_2O_3	14.04	14.20	13.90	14.05	14.52	14.70	14.72	14.84	14.50	14.03	14.22	13.59	13.67
Fe_2O_3	0.26	0.23	0.21	0.49	0.58	0.60	0.80	0.60	0.42	0.44	0.01	0.30	0.08
FeO	2.13	2.23	2.03	1.76	1.95	3.20	2.95	3.15	2.32	2.37	2.47	2.17	2.45
MgO	1.33	1.36	1.25	1.24	1.44	2.04	1.97	2.00	1.18	1.21	1.03	1.02	1.06
CaO	2.27	2.34	2.14	2.23	2.46	3.26	3.37	3.45	2.71	2.06	2.36	2.10	2.35
Na_2O	2.71	2.77	2.71	2.87	2.73	2.38	2.22	2.29	3.16	2.59	3.04	2.74	2.92
K_2O	4.04	4.31	4.36	3.81	4.03	3.58	3.86	3.64	3.25	4.72	4.49	4.70	3.91
MnO	0.04	0.05	0.05	0.05	0.05	0.07	0.06	0.06	0.05	0.06	0.06	0.05	0.06
TiO_2	0.34	0.36	0.33	0.34	0.38	0.57	0.57	0.58	0.38	0.40	0.42	0.41	0.42
P_2O_5	0.14	0.13	0.12	0.10	0.11	0.16	0.16	0.16	0.11	0.12	0.13	0.12	0.12
LOI	1.04	1.00	0.90	1.38	0.87	0.88	0.68	0.45	1.11	1.21	0.84	0.91	0.78
Total	99.93	99.79	99.81	99.83	99.82	99.69	99.70	99.95	99.83	99.82	99.85	99.85	99.86
A/NK	1.59	1.54	1.51	1.64	1.59	1.88	1.88	1.92	1.66	1.50	1.44	1.41	1.51
A/CNK	1.08	1.05	1.06	1.13	1.09	1.07	1.05	1.06	1.06	1.07	1.00	1.01	1.03
Sc	6.72		6.18	6.07	7.64	12.16	10.39		7.64	7.82	7.01		7.73
V	37.57		33.54	37.38	44.59	64.45	62.61		34.65	35.14	35.93		38.14
Cr	36.02		34.04	29.40	34.47	51.49	46.90		24.64	26.24	15.92		13.29

(continued on next page)

Table 1 (*continued*)

Samples	Group 2												
	Guangdimiao					Xiema			Tangshi		Wawutang		
	01GD01	01GD05	01GD09	01GD18	01GD20	01XM01	01XM04	01XM12	02QSH2	02QSH6	02DM2	02DM4	02DM5
Co	6.41		5.86	6.59	7.36	10.80	10.44		6.50	6.79	5.79		5.98
Ni	22.64		19.98	21.79	19.58	23.43	23.50		12.53	13.55	7.80		5.96
Ga	17.9		16.8	16.5	16.7	18.6	18.5		17.7	17.3	16.5		16.4
Rb	259		260	270	255	167	178		236	254	261		253
Sr	122		109	116	139	206	213		115	120	108		101
Y	13.86		14.20	15.50	14.89	18.07	16.08		21.96	21.07	25.05		28.14
Zr	143		138	136	162	209	196		174	182	176		158
Nb	10.99		10.75	10.81	10.02	9.42	9.22		11.33	11.88	12.37		12.80
Cs	21.63		24.04	27.82	24.88	13.80	13.55		29.62	31.53	38.81		42.29
Ba	455		422	382	466	600	798		266	489	377		287
La	36.93		34.18	30.74	38.63	39.68	34.72		38.26	38.69	26.44		32.29
Ce	69.41		64.05	58.68	71.55	70.43	61.98		70.06	73.00	51.32		64.10
Pr	7.67		7.23	6.54	7.98	7.71	6.74		7.80	7.94	5.86		7.42
Nd	26.11		24.49	22.64	26.46	27.06	24.05		27.21	27.67	21.28		26.10
Sm	4.54		4.41	4.20	4.54	5.04	4.42		5.33	5.08	4.91		5.70
Eu	0.69		0.66	0.65	0.75	1.03	0.97		0.72	0.78	0.76		0.76
Gd	4.15		3.77	3.62	3.95	4.71	3.94		4.80	4.93	4.83		5.41
Tb	0.51		0.50	0.47	0.49	0.66	0.56		0.75	0.73	0.78		0.91
Dy	2.65		2.67	2.74	2.62	3.48	3.12		4.18	4.03	4.45		5.19
Ho	0.52		0.49	0.53	0.52	0.69	0.58		0.76	0.81	0.92		1.07
Er	1.28		1.38	1.47	1.50	1.82	1.64		2.29	2.16	2.61		2.99
Tm	0.18		0.19	0.24	0.20	0.25	0.24		0.35	0.33	0.41		0.48
Yb	1.16		1.31	1.51	1.43	1.62	1.50		2.12	2.02	2.38		2.90
Lu	0.17		0.19	0.23	0.21	0.24	0.22		0.31	0.30	0.37		0.46
Hf	3.88		4.04	4.04	4.48	5.37	4.91		4.86	4.88	4.29		4.04
Ta	1.66		1.91	1.73	1.36	0.88	0.86		1.55	1.51	1.72		2.05
Pb	40.5		41.5	52.6	48.3	32.0	32.7		38.1	44.4	37.6		135
Th	27.5		25.3	30.3	47.9	19.9	17.0		28.5	27.8	20.1		29.3
U	4.71		7.94	7.54	5.96	3.75	3.00		9.72	10.02	5.88		8.01

LOI: loss ion ignition, A/CNK: molar $Al_2O_3/(CaO+Na_2O+K_2O)$; A/NK: molar $Al_2O_3/(Na_2O+K_2O)$.

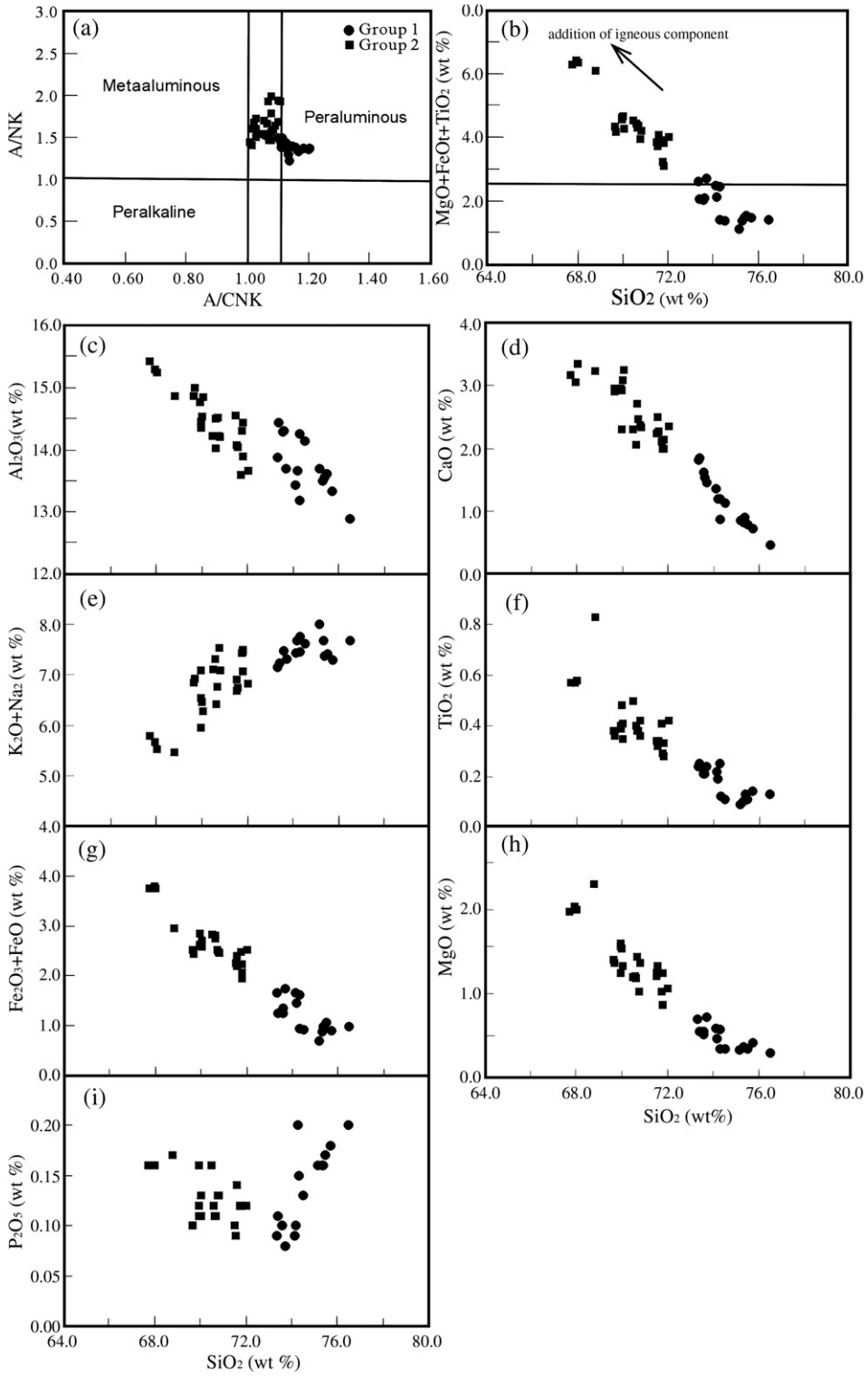

Fig. 2. (a) A/NK versus A/CNK; and SiO_2 versus (b) MgO + FeOt + TiO_2; (c) Al_2O_3; (d) CaO; (e) $K_2O + Na_2O$; (f) TiO2; (g) Fe_2O_3 + FeO; (h) MgO; (i) P_2O_5 for the Indosinian granites in Hunan Province. Symbols in (b)–(i) are the same as those in (a).

$100Fe^{3+}/(Fe^{2+}+Fe^{3+})<20$. They possess 73.3–76.5% SiO_2, 7.24–8.01% K_2O+Na_2O, 0.70–1.66% FeOt, 0.29–0.70% MgO, 0.09–0.25% TiO_2 and 0.08–0.20% P_2O_5. These samples have $K_2O>Na_2O$ and $TiO_2+FeOt+MgO<2.5$ wt.% (Fig. 2b), roughly similar to those of Himalayas leucogranites (Inger and Harris, 1993). CIPW-normative calculation gives 33.2–44.1 vol.% Qz, 22.4–29.2 vol.% Or, 22.1–30.8 vol.% Ab, 1.1–8.6 vol.% An and >1.0 vol.% corundum. Such characteristics are consistent with those of the S-type granites. In the An–Or–Ab diagram (no shown), they plot in the field of granite and are herein grouped as Group 1.

The samples from the Baimianshan, Wawutang, Chongyangping, Guandimiao, Xiangzikou, Tangshi and Xiema plutons have SiO_2 of 68.3–72.0%. A/CNK=1.0–1.1 and $TiO_2+FeOt+MgO=2.5–8.0\%$ (Fig. 2a–b). FeOt, Al_2O_3, MgO, CaO and TiO_2 are generally higher but K_2O+Na_2O is lower than those of Group 1 (Table 1). These samples are classified as granite and granodiorite (no shown), and have the modal composition of Qz=23.7–33.2 vol.%, Or=18.4–28.3 vol.%, Ab=19.0–

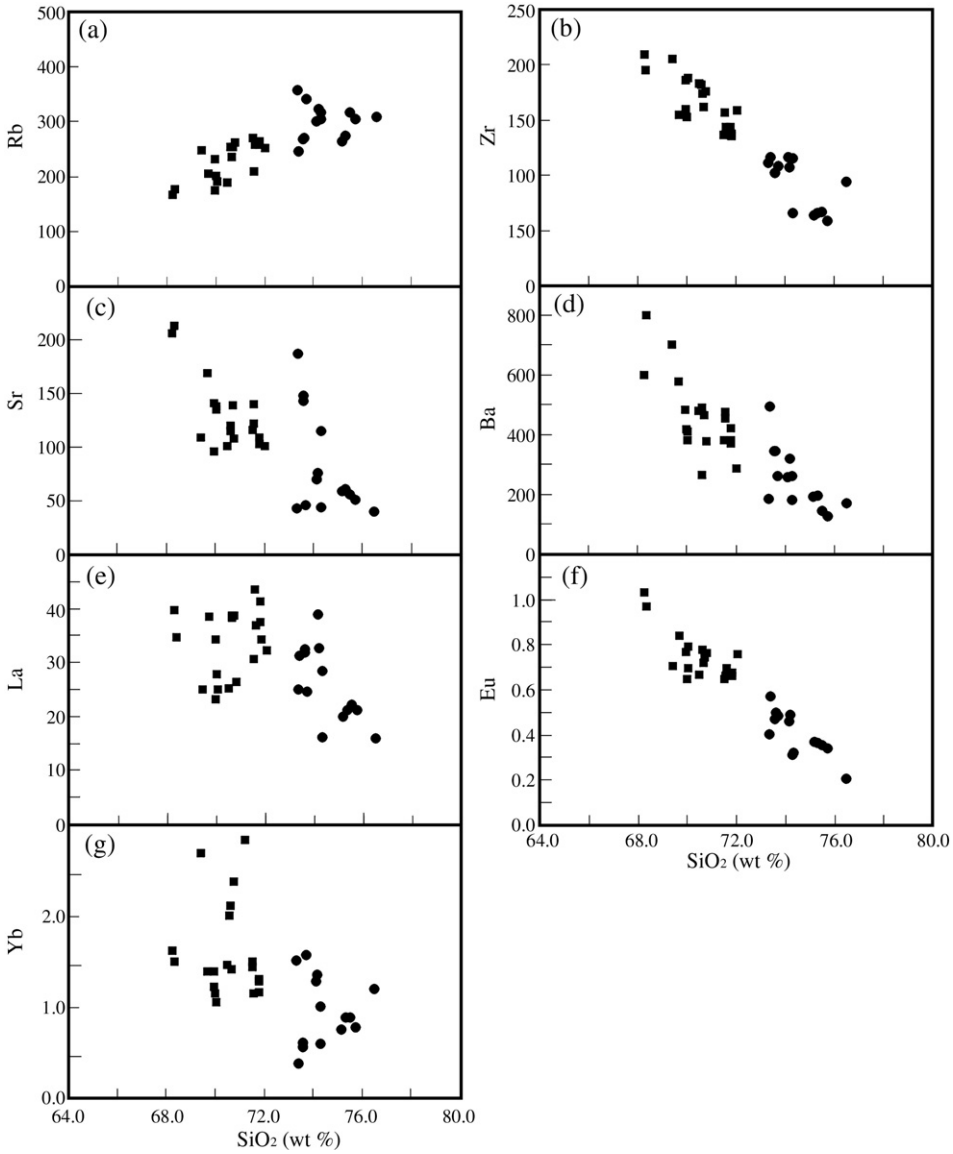

Fig. 3. Plots of SiO_2 versus (a) Rb, (b) Zr, (c) Sr, (d) Ba, (e) La, (f) Eu, (g) Yb and (h) Eu/Eu* for the Indosinian granites in Hunan Province. Symbols are the same as those in Fig. 2a.

27.6 vol.% and An=9.3–18.2 vol.%. Corundum is less than 1.0 vol.% for most samples. Such characteristics indicate an affinity to I-type granites, and we herein group these rocks as Group 2.

In Harker diagrams, all these samples exhibit significant negative correlation of Al_2O_3, MgO, CaO, TiO_2 and FeOt, but positive correlation of K_2O+Na_2O with SiO_2 (Fig. 2c–h). P_2O_5 is positively correlated with SiO_2 for Group 1 but negatively correlated with SiO_2 for Group 2 (Fig. 2i). Rb, Zr, Sr, Ba and Eu decrease but Yb shows irregular variations with increasing SiO_2 for Groups 1 and 2 (Fig. 3a–f). Rb and Ba are more enriched relative to Sr, and Rb/Sr and Rb/Ba ratios (1.81–5.96 and 0.70–2.42) are higher in Group 1 than those of Group 2 (0.81–2.52 and 0.35–0.89, respectively).

Chondrite-normalized REE patterns are shown in Fig. 4a. All the samples generally show similar pattern with difference in abundances. They have total REE content of 66–181 ppm, and are moderately to highly LREE enrichment, with $(La/Yb)n=3.9–58.2$. These granites show prominently negative Eu anomalies ($Eu/Eu^*=0.17–0.69$) and moderately HREE fractionation with $(Gd/Yb)n=1.0–4.9$. Group 1 has higher LREE/

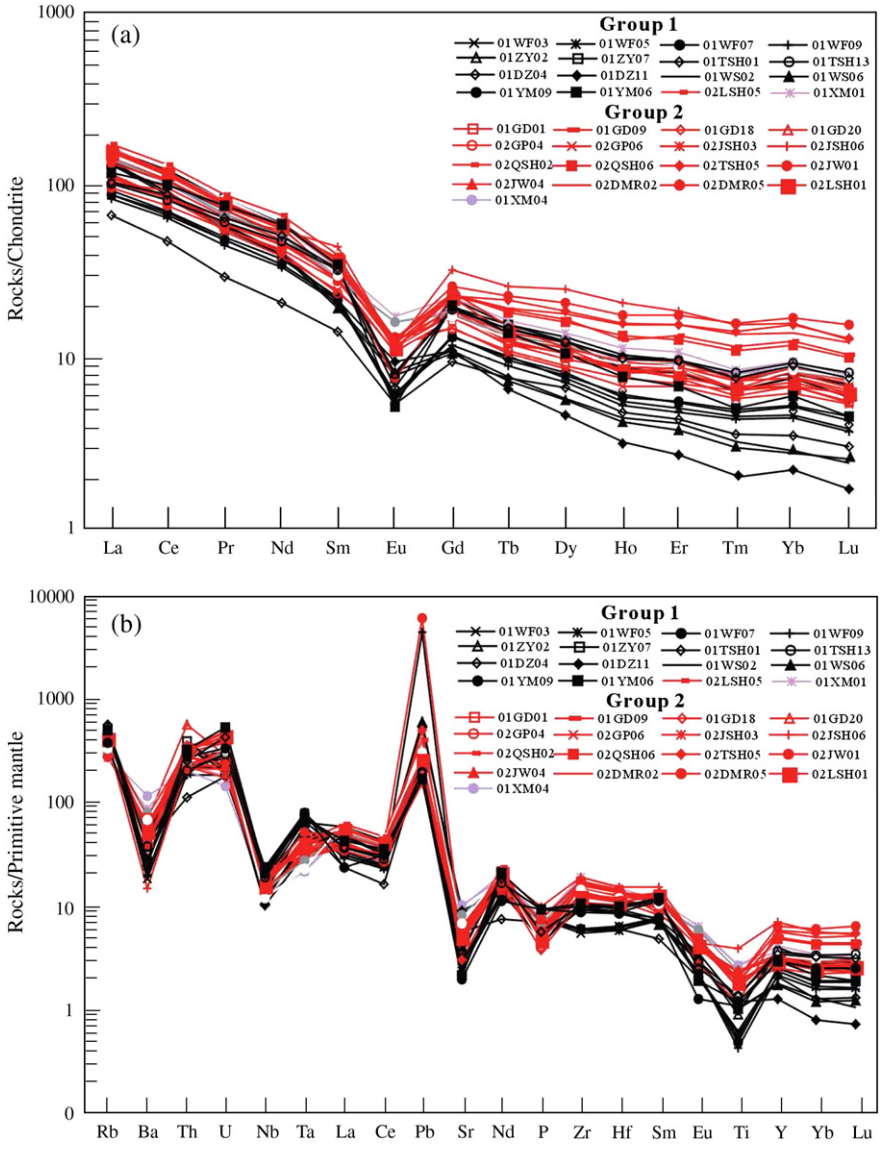

Fig. 4. (a) Chondrite-normalized REE and (b) primitive mantle-normalized trace element patterns for the Indosinian granites in Hunan Province. Normalized values for chondrite and primitive mantle are from Taylor and McLennan (1985), and Sun and McDonough (1989), respectively.

Table 2
Sr–Nd isotopic analyses for the Indosinian peraluminous granites in Hunan Province

Sample	Sm	Nd	Rb	Sr	$^{147}Sm/^{144}Nd$	$^{87}Rb/^{86}Sr$	$^{143}Nd/^{144}Nd$ (2σ)	$^{87}Sr/^{86}Sr$ (2σ)	$^{87}Sr/^{86}Sr(t)$	$\varepsilon_{Nd}(t)$	T_{DM} (Ga)
Group 1											
01WF03	3.26	16.38	305.18	51.23	0.120	17.27	0.512049 (6)	0.790183 (13)	0.733684	−9.25	1.80
01WF07	3.26	16.16	274.47	61.34	0.122	12.97	0.511998 (6)	0.766289 (14)	0.723852	−10.30	1.92
01ZY02	4.84	24.12	323.62	76.10	0.121	12.33	0.512015 (5)	0.760191 (17)	0.719858	−9.95	1.88
01ZY07	5.45	28.29	301.28	70.42	0.117	12.40	0.511964 (6)	0.761760 (14)	0.721183	−10.81	1.87
01TSH1	4.95	24.10	256.84	43.41	0.124	17.15	0.512020 (6)	0.786803 (13)	0.7306841	−9.93	1.93
01TSH13	4.80	22.31	340.60	85.60	0.130	11.54	0.512066 (7)	0.767008 (20)	0.729269	−9.21	1.98
01YM06	5.22	27.66	317.45	83.81	0.114	10.98	0.512015 (13)	0.763518 (18)	0.727594	−9.74	1.74
Group 2											
01XM01	5.04	27.06	166.57	206.14	0.113	2.34	0.512089 (5)	0.721414 (12)	0.713751	−8.25	1.61
01XM04	4.42	24.05	177.76	212.77	0.111	2.42	0.512113 (5)	0.721681 (10)	0.713758	−7.74	1.55
02JSH3	4.14	24.54	231.32	141.50	0.102	4.74	0.512083 (7)	0.730854 (18)	0.715349	−8.06	1.46
02QSH2	5.33	27.21	236.12	114.91	0.119	5.96	0.512107 (7)	0.731357 (16)	0.711870	−8.07	1.68
02QSH6	5.08	27.67	254.50	120.30	0.111	6.13	0.512083 (6)	0.732028 (13)	0.711964	−8.31	1.59
02DM02	4.91	21.28	261.21	107.71	0.140	7.03	0.512195 (5)	0.733638 (16)	0.710639	−6.96	1.97
02DM05	5.70	26.10	252.95	128.58	0.132	5.71	0.512211 (6)	0.731422 (22)	0.712763	−6.43	1.76
01GD01	4.54	26.11	259.03	121.65	0.105	6.17	0.511980 (5)	0.737591 (13)	0.717397	−10.16	1.65
01GD20	4.54	26.46	254.99	138.75	0.104	5.33	0.512012 (5)	0.732624 (13)	0.715194	−9.49	1.58

HREE ratios and more significant HREE fractionation in comparison with those of Group 2 (Fig. 4a). On primitive mantle-normalized spidergram (Fig. 4b), these samples exhibit strongly negative Ba, Sr, Nb, P and Ti anomalies and positive Pb anomalies, roughly similar to that of the sedimentary rocks in the SCB (Shen et al., 1998; Chen and Jahn, 1998; Wang et al., 2003a).

The $^{86}Sr/^{88}Sr$ and $^{146}Nd/^{144}Nd$ ratios and the analytical errors are reported in Table 2 and shown in Fig. 5. Group 1 has initial $^{87}Sr/^{86}Sr$ ratios from 0.7190 to 0.7325 and $\varepsilon_{Nd}(t)$ values from −9.2 to −10.8, similar to those of the Precambrian metasedimentary rocks from the SCB (Shen et al., 1998; Li, 1994) and Ordovician sedimentary rocks from the Lachlan Fold Belt (e.g., Healy et al., 2004). T_{DM} model ages are in the range of 1.74–1.98 Ga. Group 2 exhibits lower initial $^{87}Sr/^{86}Sr$ ratios (0.7101–0.7170) but higher $\varepsilon_{Nd}(t)$ values (−6.4–−9.4 with the exception of 01GD-01) than those of Group 1, similar to S-type granites from the Lachlan Fold Belt interpreted as the product of bulk mixing of crust-with mantle-derived components (Healy et al., 2004). T_{DM} values range from 1.76 Ga to 1.46 Ga except for the 02DM02 sample (T_{DM}=1.97).

5. Zircon U–Pb geochronological results

Six samples (01YM03 and 01WF09 from Group 1, and 02JSH03, 02DM05, 02QSH06 and 01GD09 from Group 2) were selected for SHRIMP zircon U–Pb dating and two samples (01XM01 and 02LSH05 from Group 2) were analyzed by LA-ICPMS. They are porphyritic biotite monzonitic granites with the major minerals of feldspar, plagioclase, quartz and biotite. The mineral compositions and sampling locations are shown in Background Dataset 1 and Fig. 1b. Zircon separates from these samples generally exhibit similar morphology, mostly euhedral and up to 150–350 μm in length with ~2:1–4:1 of length/width ratio. Most crystals are light brown or brown, prismatic and transparent to subtransparent, and exhibit the internal structure with strong oscillatory zoning, similar to that of typical magmatic zircons.

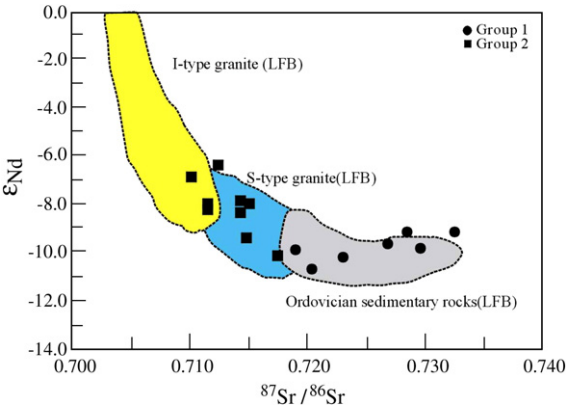

Fig. 5. Initial Sr–Nd isotopic composition of the Indosinian granites in Hunan Province compared with the Ordovician sedimentary rocks, S- and I-type granites from the Lachan Fold Belt (LFB) are from Healy et al. (2004). Symbols are the same as those in Fig. 2a.

Table 3
SHRIMP zircon U–Pb analyses for representative granites from Hunan Province

Spot	U (ppm)	Th (ppm)	$^{232}Th/^{238}U$	ppm $^{206}Pb^*$	$^{238}U/^{206}Pb^*$	$^{207}Pb^*/^{206}Pb^*$ ± %	$^{207}Pb^*/^{235}U$ ± %	$^{206}Pb^*/^{238}U$ ± %	disco (%)	$^{206}Pb/^{238}U$ ± 1σ (Ma)
01YM03: Yangmingshan pluton (group 1)										
HD1.1	4627	190	0.04	156	25.52	0.0497±2.6	0.266±3.8	0.0387±2.7	−35	245.1±6.6
HD2.1	578	165	0.29	17.5	28.34	0.0449±7.5	0.216±8.0	0.0349±2.9	463	221.0±6.4
HD3.1	1723	75	0.05	139	10.66	0.0599±1.7	0.773±3.3	0.0936±2.9	4	577±16
HD4.1	876	76	0.09	29.4	25.59	0.0517±4.1	0.277±5.0	0.0389±2.8	9	245.9±6.8
HD5.1	1018	146	0.15	33.9	25.82	0.0481±4.3	0.255±5.2	0.0385±2.8	−135	243.4±6.7
HD6.1	97	222	2.36	7.65	10.94	0.0578±12	0.716±13	0.0898±3.2	−6	554±17
HD7.1	2300	85	0.04	73.5	26.88	0.05002±1.8	0.2561±3.4	0.0371±2.9	−20	235.1±6.6
HD8.1	5110	111	0.02	169	25.94	0.05076±1.2	0.2693±3.0	0.0385±2.7	−6	243.4±6.5
HD9.1	1220	48	0.04	39.4	26.59	0.0471±4.5	0.242±5.3	0.0373±2.8	−329	235.9±6.5
HD10.1	539	146	0.28	16.9	27.45	0.0420±11	0.207±12	0.0358±2.9	201	226.5±6.5
HD11.1	402	122	0.31	31.2	11.04	0.0588±3.5	0.729±4.5	0.0899±2.8	1	555±15
HD12.1	226	151	0.69	28.3	6.85	0.0632±4.3	1.259±5.2	0.1444±3.0	−21	869±24
HD13.1	521	212	0.42	16.5	27.20	0.0454±8.8	0.226±9.4	0.0362±3.2	734	229.0±7.2
HD14.1	3064	1920	0.65	245	10.72	0.0574±0.9	0.737±2.9	0.0931±2.7	−14	574±15
HD15.1	1956	104	0.05	67.8	24.79	0.0485±2.4	0.269±3.7	0.0402±2.8	−102	254.1±6.9
HD16.1	552	99	0.19	17.3	27.43	0.0519±5.8	0.259±6.5	0.0362±2.9	18	229.1±6.5
HD17.1	1345	52	0.04	44.7	25.83	0.0483±4.0	0.256±4.8	0.0384±2.8	−115	243.2±6.7
01WF09: Wufengxian pluton (group 1)										
HF1.1	1438	3345	2.40	46.2	26.71	0.0478±3.9	0.245±4.8	0.0372±2.8	−159	235.2±6.5
HF2.1	864	152	0.18	71.1	10.43	0.0638±1.8	0.841±3.3	0.0956±2.8	20	588±16
HF3.1	607	163	0.28	88.0	5.93	0.0715±1.6	1.659±3.2	0.1682.83±	−3	1003±26
HF4.1	1289	830	0.66	41.8	26.51	0.0477±9.3	0.240±9.7	0.03652.9±	−169	231.1±6.5
HF5.1	661	1388	2.17	21.2	26.76	0.0527±9.7	0.265±10	0.0364±2.9	27	230.7±6.7
HF6.1	3916	493	0.13	131	25.72	0.0505±1.6	0.2699±3.2	0.0388±2.7	−13	245.3±6.6
HF7.1	818	353	0.45	40.6	17.31	0.0531±3.5	0.421±4.8	0.0574±3.3	−8	360±11
HF8.1	1076	297	0.29	70.3	13.15	0.0584±1.9	0.610±3.4	0.0758±2.8	13	471±13
HF9.1	158	49	0.32	65.1	2.09	0.1791±1.1	11.81±3.2	0.478±3.0	5	2520±62
HF10.1	364	156	0.44	103	3.028	0.1527±1.0	6.93±3.0	0.3293±2.8	23	1835±45
HF11.1	132	59	0.46	7.13	15.88	0.0500±20	0.423±21	0.0609±3.7	−81	381±14
HF12.1	306	41	0.14	40.4	6.52	0.0727±2.6	1.527±3.8	0.1524±2.8	9	914±24
HF13.1	1064	760	0.74	65.6	13.93	0.0528±3.1	0.519±4.2	0.0713±2.8	−39	444±12
HF14.1	728	91	0.13	33.0	18.96	0.0524±16	0.348±17	0.0481±3.4	0	303±10
02JSH03, Baimashan pluton (group 2)										
HA1.1	3292	856	0.27	110	25.64	0.05198±1.4	0.2796±2.7	0.0390±2.4	13	246.7±5.7
HA2.1	1360	407	0.31	48.6	25.18	0.1145±3.8	0.6270±4.5	0.0397±2.4	87	251.1±6.0
HA3.1	1691	474	0.29	55.5	26.26	0.0698±4.3	0.3670±5.0	0.0381±2.5	74	241.0±6.0
HA4.1	2212	460	0.21	74.2	25.68	0.0518±1.8	0.2780±3.0	0.0389±2.4	11	246.3±5.7
HA5.1	3102	821	0.27	106	25.14	0.0527±1.5	0.2890±2.8	0.0398±2.3	20	251.5±5.8
HA6.1	2558	904	0.37	83.0	26.53	0.0518±1.6	0.2691±2.8	0.0377±2.4	14	238.5±5.5
HA7.1	2464	675	0.28	86.6	24.51	0.0513±1.7	0.2884±2.9	0.0408±2.4	−2	253.8±6.0
HA8.1	2032	565	0.29	65.8	26.60	0.0582±1.8	0.3019±3.0	0.0376±2.4	56	237.9±5.5
HA9.1	2100	488	0.24	69.8	25.93	0.0548±2.2	0.2916±3.2	0.0386±2.4	40	244.0±5.7
HA10.1	2132	1157	0.56	72.6	25.42	0.0889±1.8	0.4820±3.0	0.0393±2.4	82	248.8±5.8
HA11.1	1257	412	0.34	41.2	26.26	0.0541±2.3	0.2840±3.3	0.0381±2.4	36	240.9±5.7
HA11.2	2088	524	0.26	68.9	26.05	0.0523±1.6	0.2768±2.9	0.0384±2.4	19	242.8±5.6
HA12.1	4552	1148	0.26	153	25.58	0.0553±1.1	0.2981±2.6	0.0391±2.3	42	247.2±5.7
HA13.1	1887	772	0.42	64.4	25.30	0.0733±2.1	0.3990±3.2	0.0396±2.4	76	249.9±5.8
HA14.1	3876	1223	0.33	128	25.98	0.0603±1.3	0.3099±2.7	0.0385±2.3	60	243.5±5.6
HA15.1	1598	550	0.36	57.3	24.15	0.1243±4.1	0.7100±4.8	0.0414±2.4	87	261.5±6.1
HA16.1	2815	1721	0.63	95.3	25.42	0.0557±1.6	0.3023±2.8	0.0393±2.4	44	248.7±5.7
HA17.1	2612	620	0.25	92.4	24.44	0.0939±2.0	0.5300±3.1	0.0409±2.4	83	250.5±6.0

(continued on next page)

Table 3 (*continued*)

Spot	U (ppm)	Th (ppm)	$^{232}Th/^{238}U$	ppm $^{206}Pb^*$	$^{238}U/^{206}Pb^*$	$^{207}Pb^*/^{206}Pb^*$ ± %	$^{207}Pb^*/^{235}U$ ± %	$^{206}Pb^*/^{238}U$ ± %	disco (%)	$^{206}Pb/^{238}U$ ± 1σ (Ma)
02DM05, Wawutang pluton (group 2)										
HB-1.1	3268	884	0.28	108	26.01	0.0506±1.5	0.268±2.8	0.0389±2.3	−8	242.8±5.6
HB-2.1	2071	1435	0.72	65.6	27.13	0.0530±1.7	0.269±2.9	0.0368±2.4	29	233.0±5.4
HB-3.1	458	729	1.64	13.7	28.81	0.0529±3.8	0.252±4.5	0.0346±2.5	32	219.1±5.4
HB-4.1	2150	237	0.11	68.7	26.89	0.0530±1.4	0.2719±2.8	0.0372±2.4	29	235.5±5.5
HB-5.1	2037	558	0.28	66.2	26.43	0.0495±2.0	0.2575±3.1	0.0376±2.4	−41	239.0±5.5
HB-6.1	1106	584	0.55	36.0	26.39	0.0486±4.1	0.253±4.8	0.0377±2.4	−85	238.8±5.7
HB-7.1	1088	283	0.27	33.3	28.10	0.0524±3.5	0.257±4.2	0.0355±2.4	26	225.0±5.3
HB-8.1	726	213	0.30	22.7	27.41	0.0522±3.6	0.261±4.3	0.0363±2.5	21	230.0±5.5
HB-9.1	1564	851	0.56	48.4	27.77	0.0497±3.4	0.246±4.1	0.0359±2.4	−26	227.0±5.4
HB-10.1	3566	719	0.21	121	25.26	0.0529±1.2	0.289±2.7	0.0395±2.3	23	250.0±5.7
HB-11.1	1638	639	0.40	54.1	26.04	0.0509±1.7	0.269±2.9	0.0384±2.4	−2	242.6±5.7
HB-12.1	3939	1354	0.36	130	25.94	0.05137±1.1	0.2730±2.6	0.0385±2.3	5	243.8±5.6
HB-13.1	2401	709	0.31	73.4	28.09	0.04917±2.0	0.2410±3.1	0.0355±2.4	−44	225.2±5.2
HB-14.1	2508	994	0.41	86.5	24.91	0.05059±1.5	0.2795±2.8	0.0401±2.4	−14	253.3±5.9
02QSH06, Tangshi pluton (group 2)										
HC1.1	1589	389	0.25	50.5	27.09	0.0488±2.4	0.2481±3.7	0.0369±2.8	−72	233.7±6.4
HC2.1	3811	799	0.22	131	25.08	0.0495±1.5	0.2720±3.1	0.0399±2.7	−48	252.1±6.8
HC3.1	3133	598	0.20	104	25.88	0.0503±2.0	0.2680±3.4	0.0386±2.7	−17	244.4±6.6
HC4.1	4918	839	0.18	176	24.11	0.0503±1.2	0.2877±3.0	0.0415±2.7	−25	262.0±7.0
HC5.1	3148	546	0.18	107	25.38	0.0493±1.6	0.2676±3.2	0.0394±2.8	−56	249.1±6.7
HC6.1	4866	552	0.12	170	24.81	0.0490±2.6	0.2720±3.8	0.0403±2.8	−72	254.7±6.9
HC7.1	1758	406	0.24	58.0	26.23	0.0499±2.5	0.2621±3.7	0.0381±2.8	−28	241.2±6.5
HC8.1	5212	765	0.15	191	23.47	0.0506±1.4	0.2972±3.0	0.0426±2.7	−21	269.0±7.2
HC9.1	4337	852	0.20	168	23.56	0.0584±6.7	0.3020±7.2	0.0424±2.8	51	267.8±7.3
HC10.1	2866	519	0.19	95.2	26.56	0.0523±4.7	0.2720±5.4	0.0377±2.8	21	238.3±6.5
HC10.2	2175	417	0.20	69.8	27.06	0.0482±3.8	0.2450±4.7	0.0370±2.8	−118	233.9±6.4
HC11.1	2125	440	0.21	69.5	26.68	0.0499±4.1	0.2580±5.0	0.0375±2.8	−25	237.2±6.4
HC12.1	3032	444	0.15	105	24.94	0.0489±1.6	0.2704±3.2	0.0401±2.8	−76	253.4±6.8
HC13.1	1556	565	0.38	51.5	26.12	0.0483±3.2	0.2550±4.2	0.0383±2.8	−117	242.2±6.6
HC14.1	1735	626	0.37	59.2	25.30	0.0486±2.4	0.2647±3.7	0.0395±2.8	−98	249.9±6.8
HC15.1	1858	611	0.34	64.8	24.76	0.0503±2.5	0.2800±3.8	0.0404±2.8	−23	255.3±6.9
HC16.1	2896	589	0.21	99.3	25.09	0.0514±1.6	0.2822±3.2	0.0399±2.7	2	252.0±6.8
HC17.1	3952	639	0.17	121	28.46	0.0492±3.3	0.2380±4.3	0.0351±2.8	−43	222.6±6.0
01GD09: Guandimiao pluton (group 2)										
HE1.1	1029	356	0.36	33.4	26.64	0.0486±4.7	0.2510±5.5	0.0375±2.8	−88	237.5±6.6
HE2.1	1168	605	0.54	38.8	26.12	0.0505±4.3	0.2670+5.1	0.0383±2.8	−11	242.2±6.7
HE3.1	925	640	0.71	29.1	27.55	0.0506±4.5	0.2531±5.3	0.0363±2.8	−3	229.9±6.4
HE4.1	6157	13044	2.19	24.8	21.48	0.0516±2.2	0.3310±3.8	0.0466±3.1	−10	293.4±9.0
HE5.1	1139	610	0.55	38.6	25.61	0.0455±5.1	0.2451±5.8	0.0390±2.8	1003	246.9±6.8
HE6.1	475	315	0.69	14.9	27.9	0.0463±11	0.2290±11	0.0359±3.7	−1560	227.1±8.2
HE7.1	2148	1256	0.60	73.8	25.21	0.0478±3.3	0.2610±4.3	0.0397±2.8	−183	250.8±6.8
HE8.1	1539	1218	0.82	51.2	26.16	0.0490±4.4	0.2581±5.2	0.0382±2.8	−65	241.8±6.6
HE9.1	721	502	0.72	22.8	27.49	0.0453±8.1	0.2270±8.5	0.0364±2.9	654	230.3±6.5
HE101	804	488	0.63	26.6	26.19	0.0477±5.4	0.2510±6.1	0.0382±2.8	−192	241.5±6.7
HE11.1	1803	808	0.46	61.9	25.09	0.0492±2.4	0.2706±3.7	0.0399±2.8	−58	252.0±6.8
HE12.1	1348	841	0.64	44.3	26.27	0.0530±2.9	0.2781±4.0	0.0381±2.8	27	240.8±6.6
HE12.2	1221	598	0.51	40.0	26.44	0.0496±4.2	0.2590±5.0	0.0378±2.8	−35	239.4±6.6
HE13.1	1879	845	0.46	63.8	25.46	0.0500±2.8	0.2700±4.0	0.0393±2.8	−29	248.4±6.8
HE14.2	1418	1082	0.79	47.9	25.63	0.0492±3.9	0.2650±4.8	0.0390±2.8	−59	246.8±6.8

5.1. SHRIMP zircon U–Pb dating results

The analytical data are listed in Table 3, and presented in Fig. 6.

5.1.1. Yangmingshan pluton (01YM03)

As shown in Fig. 6a, the 16 analyses form two clusters except that analytical spot of HD12.1 gives an $^{206}Pb/^{238}U$ age of 869±24 Ma. One cluster defined

by four analyses gives a weighted mean $^{206}Pb/^{238}U$ age of 565±16 Ma (MSWD=0.60), interpreted to be inherited from the magma source. The others yield a weighted mean $^{206}Pb/^{238}U$ age of 237±5 Ma (MSWD=1.3), representing the crystallization age of the pluton.

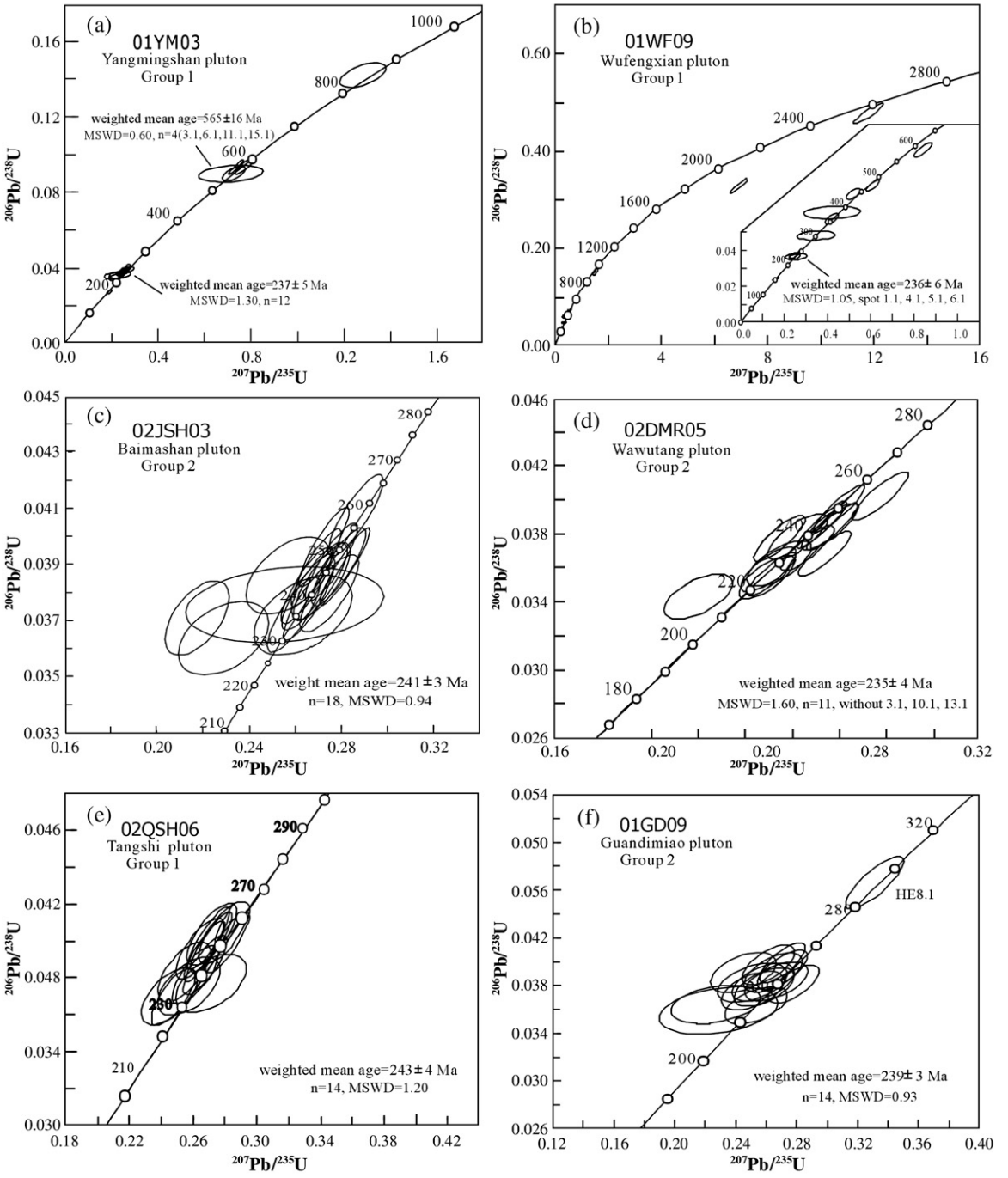

Fig. 6. Concordia diagrams of SHRIMP zircon U–Pb data for the representative granites in Hunan Province (a): 01YM03 (Yangmingshan pluton, Group 1); (b) 01WF09 (Wufengxian pluton, Group 1); (c) 02JSH03 (Baimashan pluton, Group 2); (d) 02DMR05 (Wawutang pluton, Group 2); (e) 02QSH06 (Tangshi pluton, Group 2); (f) 01GD09 (Guangdimiao pluton, Group 2).

Table 4
LA-ICPMS zircon U–Pb analyses for the representative granites from Hunan Province

	U ppm	Th (ppm)	$^{232}Th/^{238}U$	$^{206}Pb^*$ ppm	$^{207}Pb/^{206}Pb$ (±1σ)	$^{207}Pb/^{235}U$ (±1σ)	$^{206}Pb/^{238}U$ (±1σ)	$^{207}Pb/^{206}Pb$ ± 1σ(Ma)	$^{207}Pb/^{235}U$ ± 1σ(Ma)	$^{206}Pb/^{238}U$ ± 1σ(Ma)
01XM-01: Xiema pluton (group 2)										
AP09D08	1226	1003	0.82	173	0.08925(88)	0.42920(397)	0.03489(33)	1410±8	363±3	221±2
AP09D10	2133	2573	1.21	320	0.05842(58)	0.26502(246)	0.03291(31)	546±9	239±2	209±2
AP09D11	921	303	0.33	128	0.05142(51)	0.24481(227)	0.03454(32)	260±10	222±2	219±2
AP09D13	743	136	0.18	105	0.06230(62)	0.30063(278)	0.03501(33)	684±9	267±2	222±2
AP09D14	698	1078	1.54	113	0.20163(199)	1.16649(992)	0.04198(39)	2839±7	785±5	265±2
AP09D15	573	134	0.23	82.4	0.05378(54)	0.24278(226)	0.03275(31)	362±10	221±2	208±2
AP09D16	1595	3106	1.95	230	0.06087(60)	0.27093(251)	0.03230(30)	635±9	243±2	205±2
AP09D17	767	184	0.24	111	0.05076(50)	0.24880(229)	0.03557(33)	230±10	226±2	225±2
AP09D18	736	302	0.41	113	0.10514(104)	0.51355(472)	0.03544(33)	1717±8	421±3	225±2
AP09D20	1388	565	0.41	202	0.05201(51)	0.25589(234)	0.03570(33)	286±10	231±2	226±2
AP09D22	799	184	0.23	117	0.05131(51)	0.24913(229)	0.03523(33)	255±10	226±2	223±2
AP09D23	1215	355	0.29	175	0.05071(50)	0.24580(224)	0.03517(33)	228±10	223±2	223±2
AP09D24	266	12	0.04	46.3	0.05026(82)	0.25367(341)	0.03661(33)	207±38	230±3	232±2
AP09D25	1431	1412	0.99	204	0.06210(61)	0.29584(270)	0.03457(32)	678±9	263±2	219±2
AP09D27	1586	393	0.25	204	0.05052(50)	0.22652(206)	0.03254(30)	219±10	207±2	206±2
AP09D28	1189	416	0.35	170	0.05210(52)	0.24678(225)	0.03437(32)	290±10	224±2	218±2
AP09D29	587	153	0.26	78.6	0.07284(72)	0.35218(321)	0.03509(32)	1010±8	306±2	222±2
AP09D31	1919	2593	1.35	271	0.06189(61)	0.29137(265)	0.03416(31)	670±9	260±2	217±2
AP09D34	850	191	0.22	120	0.04955(49)	0.23378(212)	0.03424(31)	174±10	213±2	217±2
AP09D35	1228	254	0.21	190	0.06688(68)	0.31934(298)	0.03465(32)	834±9	281±2	220±2
AP09D36	974	618	0.63	141	0.05044(145)	0.24373(658)	0.03505(35)	215±68	221±5	222±2
AP09D37	1545	401	0.26	220	0.05249(52)	0.24824(224)	0.03432(31)	307±9	225±2	218±2
AP09D38	1809	3216	1.78	284	0.05907(58)	0.27826(251)	0.03418(31)	570±9	249±2	217±2
02LSH-05: Xiangzikou pluton (group 2)										
AP09E06	1977	498	0.25	297	0.05679(104)	0.28818(451)	0.03681(35)	483±41	257±4	233±2
AP09E07	2376	614	0.26	335	0.05209 (92)	0.24320(361)	0.03386(32)	289±41	221±3	215±2
AP09E08	949	555	0.58	249	0.11550(113)	0.99701(913)	0.06268(59)	1888±8	702±5	392±4
AP09E09	4240	862	0.20	544	0.05049(5)	0.21806(202)	0.03139(29)	218±10	200±2	199±2
AP09E10	1482	305	0.21	199	0.05110(5)	0.23600(217)	0.03353(31)	245±10	215±2	213±2
AP09E12	1502	349	0.23	212	0.05429(53)	0.26019(239)	0.03480(33)	383±10	235±2	221±2
AP09E13	5404	392	0.07	747	0.05235(51)	0.24382(224)	0.03382(32)	301±10	222±2	214±2
AP09E14	1622	396	0.24	220	0.05199(51)	0.23403(215)	0.03269(31)	285±10	214±2	207±2
AP09E15	1917	464	0.24	240	0.05108(90)	0.21539(322)	0.03058(29)	245±42	198±3	196±2
AP09E16	1522	302	0.20	192	0.05704(104)	0.25120(391)	0.03194(30)	493±41	228±3	203±2
AP09E18	2433	384	0.16	373	0.05916(58)	0.30679(283)	0.03767(35)	573±9	272±2	238±2
AP09E19	1298	513	0.40	173	0.04991(49)	0.22506(207)	0.03276(31)	191±10	206±2	208±2
AP09E20	3651	1012	0.28	484	0.05492(98)	0.24521(372)	0.03238(30)	409±41	223±3	205±2
AP09E21	2189	510	0.23	299	0.05076(5)	0.23395(215)	0.03348(31)	230±10	213±2	212±2
AP09E22	2063	297	0.14	282	0.05118(5)	0.23622(218)	0.03353(31)	249±10	215±2	213±2
AP09E24	4902	385	0.08	668	0.05013(49)	0.23033(212)	0.03338(31)	201±10	210±2	212±2
AP09E25	2828	582	0.21	395	0.05011(49)	0.23581(217)	0.03419(32)	200±10	215±2	217±2
AP09E26	2118	682	0.32	303	0.05736(57)	0.27596(254)	0.03496(33)	505±9	247±2	222±2
AP09E27	2261	465	0.21	312	0.05054(50)	0.23509(217)	0.03380(32)	220±10	214±2	214±2
AP09E28	1802	406	0.23	247	0.05237(52)	0.24118(223)	0.03347(31)	302±10	219±2	212±2
AP09E30	4242	978	0.23	575	0.05327(53)	0.24268(226)	0.03311(31)	340±10	221±2	210±2
AP09E31	1897	498	0.26	278	0.05226(162)	0.24454(721)	0.03394(33)	297±73	222±6	215±2
AP09E32	1858	413	0.22	252	0.05727(57)	0.25494(236)	0.03235(30)	502±9	231±2	205±2
AP09E33	4137	1095	0.26	552	0.05365(53)	0.24022(222)	0.03254(30)	356±10	219±2	206±2

5.1.2. Wufengxian pluton (01WF09)

Four out of the 14 grains with oscillatory zoning yield a coherent age cluster with a weighted mean $^{206}Pb/^{238}U$ age of 236±6 Ma (MSWD=1.05), which is taken as the crystallization age of the granite (Fig. 6b). The remaining 11 analyses are plotted along the concordia curve and give variably apparent ages between 303 and 2520 Ma, with nearly concordant ages of 303, 360, 914, 1003 and 2520 Ma. These older zircons have cores surrounded by heterogeneously

spotted and estuary rims, possibly inherited from the magma source.

5.1.3. Baimashan pluton (02JSH03)

Eighteen analyses were carried out on 17 euhedral grains with good pyramid terminations and strong oscillatory zonations, giving a weighted mean $^{206}Pb/^{238}U$ age of 241±3 Ma (MSWD=0.94, Fig. 6c), representing the crystallization time of the pluton.

5.1.4. Wawutang pluton (01DM05)

The 14 analyses on 14 prismatic zircon grains with oscillatory zoning structure yield a coherent group with a weighted mean $^{206}Pb/^{238}U$ age of 234±4 Ma (MSWD=1.60) (Fig. 6d), representing the emplacement age of the granitic pluton.

5.1.5. Tangshi pluton (02QSH06)

Eighteen analyses on 18 zircons have 1556–4866 ppm of U, 389–852 ppm of Th, with 0.12–0.38 of Th/U ratio. The 14 analyses yield a coherent group with a weighted mean $^{206}Pb/^{238}U$ age of 243±4 Ma (n=14, MSWD=1.2; Fig. 6e). The analyses on HC4.1, HC8.1, HC9.1 and HC17.1 are not included in the above mean calculation because they have extremely high U contents.

5.1.6. Guandimiao pluton (01GD09)

Fourteen analyses have U=475–2148 ppm, Th=315–1256 ppm and Th/U=0.36–0.82, and yield a weighted mean $^{206}Pb/^{238}U$ age of 239±3 Ma (MSWD=0.93, Fig. 6f). One analytical spot (HE4.1) has extremely high Th and U contents (Th=13044 ppm, U=6157 ppm), and gives a $^{206}Pb/^{238}U$ apparent age of 293.4±9.0 Ma. This grain shows complex internal structure, probably an inherit grain.

5.2. LA-ICPMS zircons U–Pb analytical results

The analytical results of samples of two granites (01XM01 and 02LSH05) for Group 2 are presented in Table 4 and shown in Fig. 7. It shows that the distribution of analytical zircons plot on or away from the concordia curve, illustrating that some grains contain extent degree contributions of common lead, or addition and loss of U and Pb isotopes after the crystallizion. This disconcordance is commonly regarded as higher ^{207}Pb counting during measurement, which does not affect the use of $^{206}Pb/^{238}U$ ages for <1000 Ma zircons after common Pb correction. Fortunately, our zircons are younger and thus $^{206}Pb/^{238}U$ age is precise and usable.

5.2.1. Xiema pluton (01XM01)

One analytical spot (AP09D014) gives a $^{206}Pb/^{238}U$ apparent age of 265±2 Ma, interpreted as an inherited zircon. Other twenty-two analyses yield a weighted mean $^{206}Pb/^{238}U$ age of 218±3 Ma (MSWD=2.1; Fig. 7a), similar to those of Dashenshan and Taojiang plutons measured by SHRIMP zircon U–Pb method (Xu et al., 2004).

5.2.2. Xiangzikou pluton (02LSH05)

An analytical spot AP09E08 gives an older age of 392±4 Ma, indicative of an inherited zircon. Other 24 analyses yield a weighted mean $^{206}Pb/^{238}U$ age of 210±5 Ma (MSWD=2.1, Fig. 7b). This age represents the crystallization age of the pluton, consistent with the geological observation that Xiangzikou pluton intruded into the Tangshi intrusion with crystallization age of 243±4 Ma (Fig. 1b and Table 4).

Consequently, these samples gave the age-cluster of 235–243 Ma and 210–218 Ma. The apparent $^{206}Pb/^{238}U$

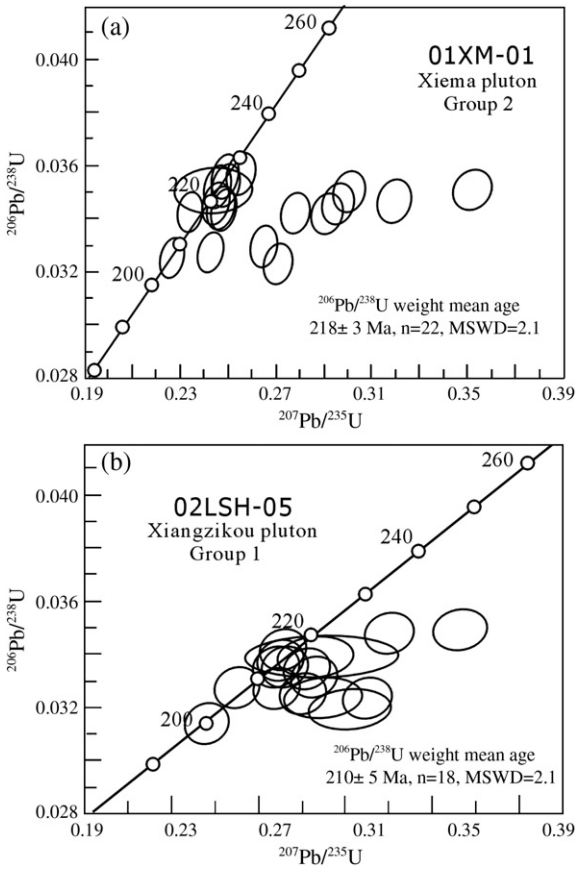

Fig. 7. Concordia diagram of LA-ICPMS zircon U–Pb data for Xiema (Group 2, 01XM01, a) and Xiangzikou (Group 2, 02LSH05, b) plutons in Hunan Province.

ages of inherited zircons varying from 265 Ma to 2520 Ma are additionally obtained.

6. Petrogenetic constraints

6.1. Emplacement conditions

Although there is no applicable mineral barometer to determine the emplacement depth of these granites, in the CIPW-normative Qz–Ab–Or diagram (Fig. 8a), most samples plot in the low-temperature field near to 5 kb, and to the right of the cotectic/eutectic minima of the H_2O saturated haplogranite system, typical of high-level emplacement of natural low temperature granites (Johannes and Holtz, 1996). The unidirectional growth of dendritic alkali feldspar also indicates a high-level emplacement of these granites.

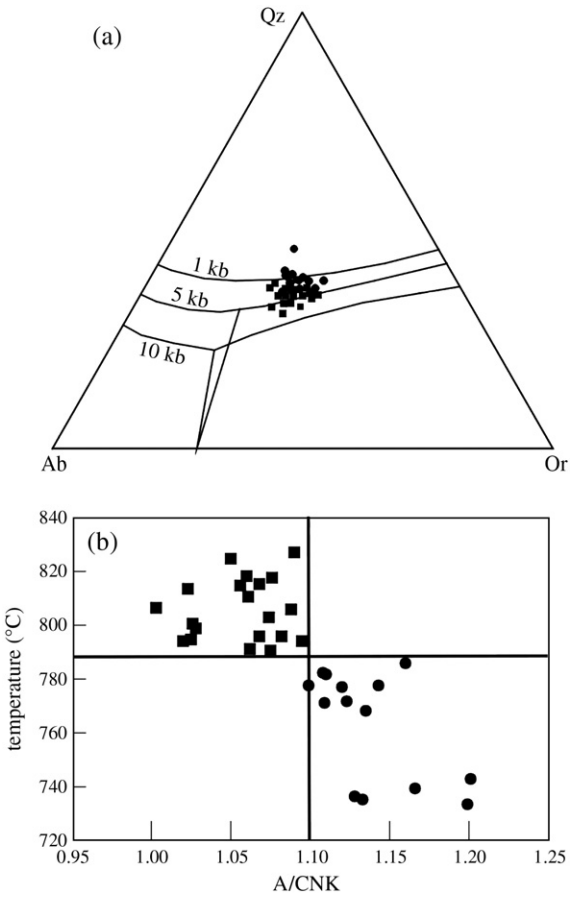

Fig. 8. (a) CIPW-normative Qz–Ab–Or diagram with low temperature melt compositions at 1, 5 and 10 kb (Johannes and Holtz, 1996); (b) plot of A/CNK and temperature (°C) calculated by zircon saturation thermometry (Watson and Harrison, 1983) of the Indosinian granites in Hunan Province.

The estimates of magma temperatures are obtained by zircon saturation thermometry (Watson and Harrison, 1983) with insignificant contribution from inherited zircons to the Zr and monazite to the LREE, respectively. The low Zr contents (<120 ppm) for Group 1 yielded an estimated temperature of 734–786 °C (Fig. 8b), which is slightly higher than that of High Himalaya leucogranites (HHL, Harris et al., 1995; Zhang et al., 2004a,b). The presence of the inherited zircons is an indicative of lower temperature for Group 1 (Watson and Harrison, 1983). This is also in agreement with insignificant contact metamorphism in the country rocks. Group 2 has Zr = 135–210 ppm and the estimated temperature ranges from 791 °C to 827 °C, slightly higher than that of Group 1 (Fig. 8b).

6.2. Potential source natures

Fractional crystallization of plagioclase, biotite, K-feldspar and zircon are certainly important for both groups, as suggested by decreasing of CaO, FeOt, MgO, TiO_2, Na_2O+K_2O, Al_2O_3, Zr, Sr and Ba with increasing SiO_2 (Figs. 2 and 3). It is obvious that the Rb–Ba and Ba–Sr variations (Fig. 9a–b) and the negative correlation between SiO_2 and Sr, Eu, Eu/Eu*, as well as strongly negative Ba, Sr, P and Ti anomalies (Fig. 4b) supported fractionation of alkaline feldspar and plagioclase. However, decreasing of Zr/Hf and Nb/Ta ratios for both groups with increasing SiO_2 (Fig. 9c–d), and the distinct Sr–Nd isotopic compositions for these samples cannot be explained by a closed-system fractional crystallization process (e.g., Dostal and Chatterjee, 2000). In contrast, these geochemical signatures might be the consequence of heterogeneous source.

All analyzed samples are peraluminous rocks, giving a first-order constraint that their sources are most likely metasedimentary/metaigneous rocks (Kalsbeek et al., 2001). The strongly peraluminous, silica-rich compositions of Group 1 suggested that the magma can be generated by (1) the partial melting of aluminous-rich metamorphic rocks (e.g., schists and gneisses); (2) the partial melting of amphibolites under H_2O-rich conditions (Ellis and Thompson, 1986); or (3) fractionation of aluminous-poor magma (Zen, 1986). However, the products from both cases (2) and (3) are usually characterized by metaluminous, Na- and Sr-rich features (Zen, 1986; Gaudemer et al., 1988), in contrary to our observations. The anatexis of the high-grade metamorphic rocks usually produce 2–5 vol.% melts under H_2O-rich conditions (Zen, 1986; Clemens and Vielzeuf, 1987; Patiño-Dounce et al., 1990), rather than

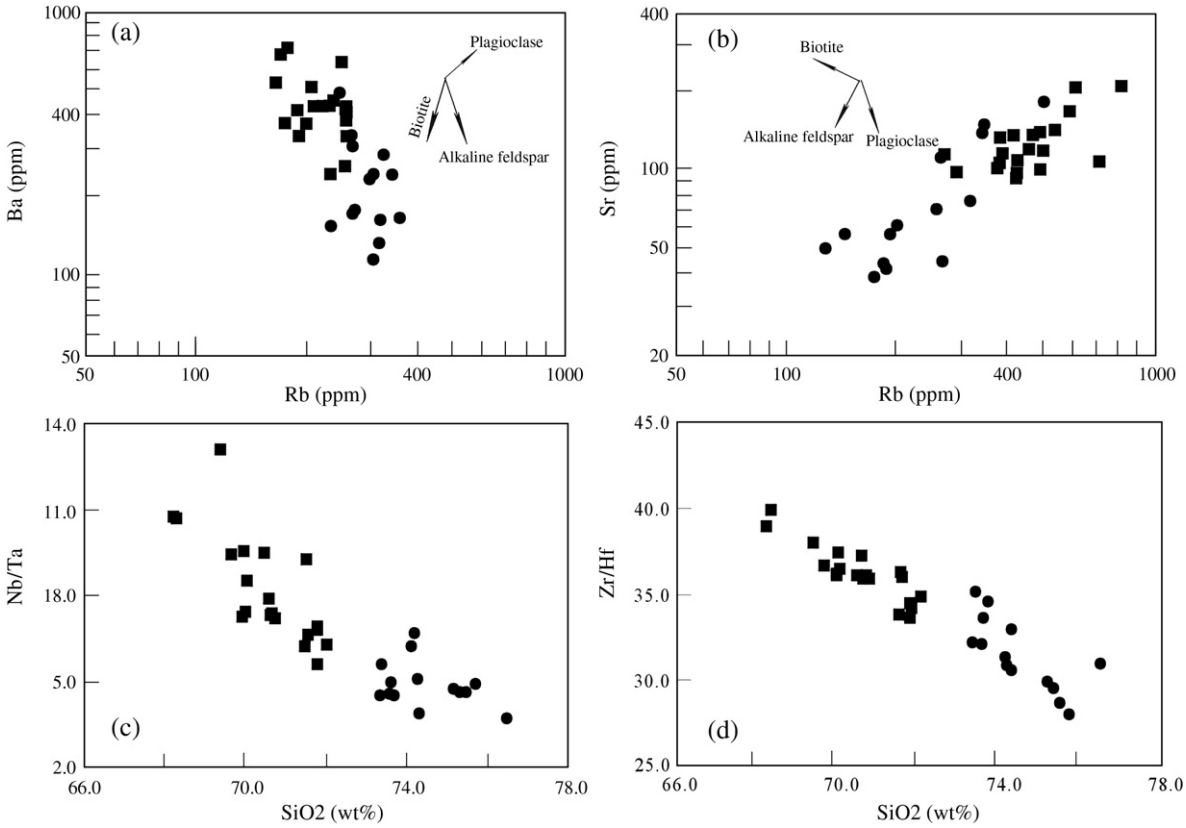

Fig. 9. Fractional crystallization vector diagrams (a: Rb–Ba and b: Ba–Sr); SiO_2 versus Nb/Ta (c) and Zr/Hf (d) for the Indosinian granites in Hunan Province. Symbols are the same as those in Fig. 2a.

voluminously peraluminous granitic batholith. Thus the Group 1 magma is most likely metasedimentary origin in the middle/upper crust. This is supported by the presence of the inherited Paleozoic and Proterozoic zircons and the T_{DM} model age (T_{DM}=1.74–1.98 Ga) for Group 1. The high Rb contents also suggest a micaceous source.

The Group 1 samples have lower CaO/Na_2O ratio than that of Group 2. In Fig. 10a, they fall in the field of the orogenic strongly peraluminous granites (Sylvester, 1998), and mostly in that of Himalayas leucogranite, while the Group 2 samples plot along a mixing line between pelite- and basalt-derived melts. Such characteristics indicate that Group 1 was derived from plagioclase-poor and clay-rich source (e.g., metapelite) whereas Group 2 was from plagioclase-rich and clay-poor source (Chappell and White, 1992; Sylvester, 1998). Higher Al_2O_3/TiO_2 ratio for Group 1 relative to Group 2 indicates that Group 2 was generated at higher temperature and pressure (Sylvester, 1998), consistent with the above estimation. The metapelitic-derived melts have commonly higher Al_2O_3/(MgO+FeOt) but lower CaO/(MgO+FeOt) ratios than those from the metaigneous rocks (Altherr et al., 2000). Group 1 exhibits similar Al_2O_3/(MgO+FeOt) ratio to that of the metasedimentary-derived melt, and Group 2 has Al_2O_3/(MgO+FeOt) <2, similar to those of metabasaltic- and metatonalitic-derived melts. The higher MgO, FeOt and TiO_2 contents and lower SiO_2 and Al_2O_3/CaO ratio for Group 2 relative to Group 1 also require the involvement of intermediate component associated with metaigneous rocks (Patiño-Dounce and Harris, 1998; Anthony, 2005).

The Group 1 samples exhibit a steep REE slope with (La/Yb)cn=9.3–58.2 and (Gd/Yb)cn=1.9–3.0 for almost samples, suggesting residual garnet in the source. Ta is decoupled from Nb, with the Nb/Ta ratios of 4.0–7.0. They are alkali-calcic, strongly peraluminous, and show significant Sr, P and Ti negative anomalies, and $\varepsilon_{Nd}(t)$ values of −9.2–−10.8, geochemically similar to mid-Tertiary granite suite of the southern Colorado Minerla Belt (Stein and Crook, 1990), an indicative of a metasedimentary source (Anthony, 2005). The Group 2 samples are magnesian,

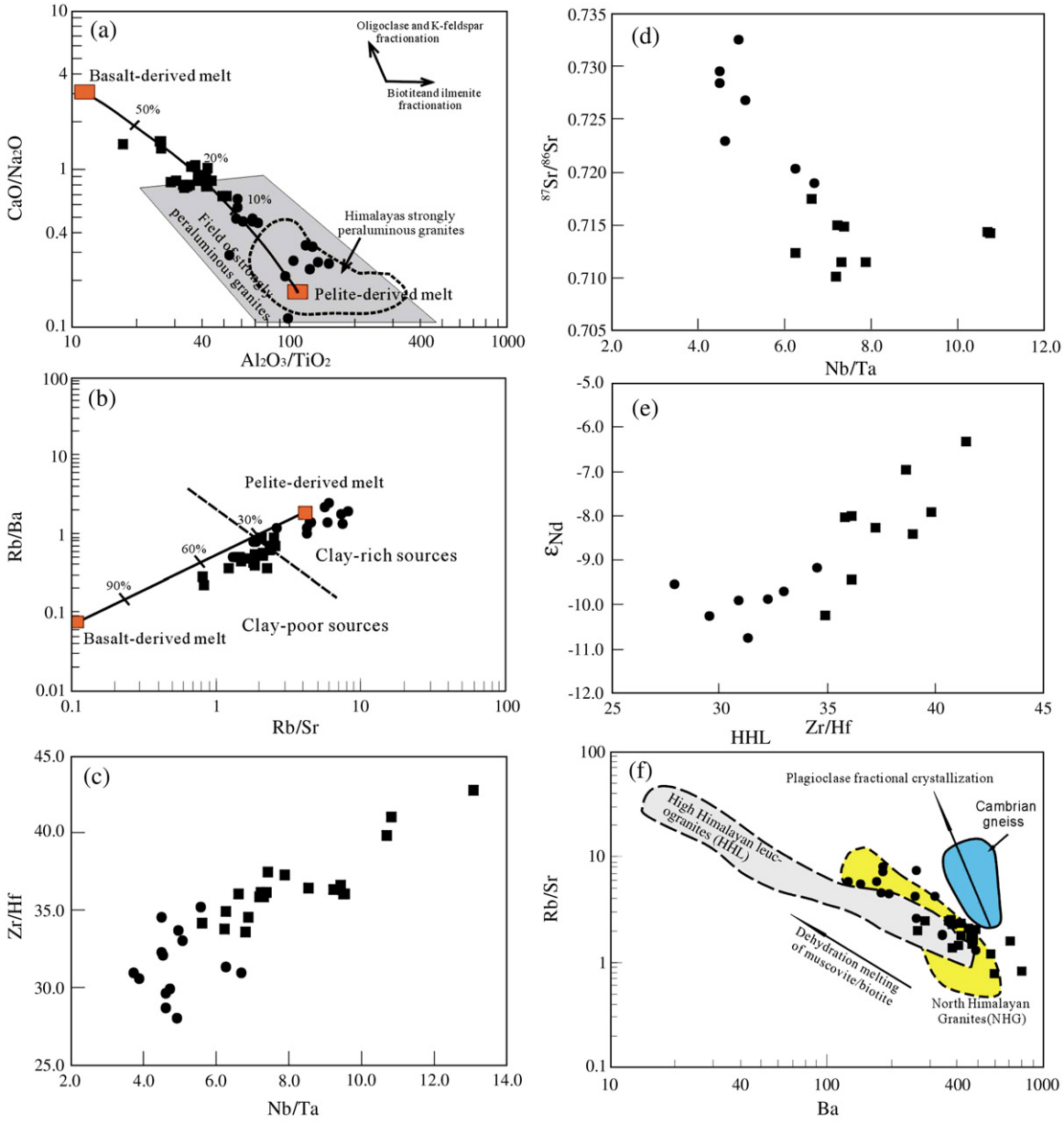

Fig. 10. Al_2O_3/TiO_2 vs. CaO/Na_2O (a), Rb/Sr vs. Rb/Ba (b), Nb/Ta vs. $^{87}Sr/^{86}Sr$ (c), Zr/Hf vs. $\varepsilon_{Nd}(t)$ (d), and Nb/Ta vs. Zr/Hf (e), and Rb/Sr vs. Ba (f) of the Indosinian granites in Hunan Province. Fields of strongkly peraluminous granites for all orogens and Himalayas are from Sylvester (1998). The mixing curve between the basalt- and pelite-derived melts in (a)–(b) is from Patiño-Dounce and Harris (1998) and Sylvester (1998). Cambrian gneiss and peraluminous granites from the North Himalayan Granites (NHG) and High Himalayan leucogranites (HHL) in (f) are from Inger and Harris (1993) and Zhang et al. (2004a,b). Symbols are the same as those in Fig. 2a.

slightly peraluminous. They dispaly a moderate REE slope with (Gd/Yb)cn = 1.5–2.5 (Fig. 4a), a shallower Ti trough (Fig. 4b) and higher $\varepsilon_{Nd}(t)$ values (−6.4–−9.4) in comparison with those of the Group 1 samples. Nb/Ta ratios range from 6.0 to 11.0 for almost samples. Such signatures are similar to those of the Laramide suite of Stein and Crook (1990), suggesting that a metabasaltic component in source reservoir might have been significant. The Rb–Sr–Ba variations of both groups are shown in Fig. 10b. These data give a linear array of increasing Rb/Sr with Rb/Ba. Consequently, Group 1 might be derived from a clay-rich source. Group 2 exhibits lower Rb/Sr but higher Sr/Ba ratios, probably indicative of mixed source with higher

plagioclase/clay ratios (Chappell and White, 1992; Jung et al., 2000).

In the diagrams of the incompatible element ratios versus isotopic compositions (Fig. 10b and c–e), the samples for both Groups 1 and 2 exhibit linear trends that suggest a binary mixing. One end-member is characterized by the metapelite-derived strongly peraluminous melt (represented by Group 1), the other is represented by the basaltic-derived melt with the relatively low SiO_2, $^{87}Sr/^{86}Sr$ and Rb/Sr, but high Ba and $FeO+MgO+TiO_2$ (Figs. 2b and 10a–b). Nb/Ta and Zr/Hf ratios decrease with increasing SiO_2 (Fig. 9c–d), also supporting such a hypothesis when the involvement of aqueous fluid phases is ruled out. Two petrogenetic models can be put forward to explain the above-mentioned geochemical features. These include that (a) the juvenile basaltic magma was underplated into the crust and some mixed with the metapelite-derived melt, and (b) metapelite- and metabasaltic-derived magmas were mixed. However, (1) newly mantle-derived melts during early Indosinian (225–245 Ma) have not been observed in the SCB; (2) the compressive regime in the SCB during early Indosinian period argues against the setting of lithospheric extension that results in underplating of the new basaltic magma (e.g., Chen, 1999; Wang et al., 2005a); (3) T_{DM} model ages are Proterozoic for Group 2, much more than Indosinian; and (4) the estimated temperature is less than 830 °C, against the direct involvement of newly mantle-derived high-temperature magma. These data suggest that the first hypothesis seems unlikely unless the lower/middle crust behaved as a very effective "density filter" to confine all of the newly mantle-derived magma at the deep levels (Jung et al., 2000; Wang et al., 2002). Consequently, we consider that the formation of Group 2 might be attributed to a mica- and epidote/zoisite-rich metavolcanoclastic source, such as metabasaltic rocks, interlayered with metasedimentary rocks whereas Group 1 was from a metapelite-dominated source. The differences in the incompatible element ratios (e.g., Rb/Sr, Sr/Ba) and REE abundances between the two groups are likely related to the distinct melting conditions and different proportions of plagioclase, muscovite, biotite, epidote/zoisite and garnet in the source (Jung et al., 2003).

In the Rb/Sr–Ba diagram (Fig. 10f), the samples from both groups show a negative correlation parallel to that of the North Himalayan Granites (NHG)/High Himalayan leucogranites (HHL) (e.g., Zhang et al., 2004a,b). Such a trend suggests that peritectic alkali feldspar was involved in the reaction since alkali feldspar is a late crystallization phase evidenced by petrographic texture. Compared with Group 2, Group 1 has higher Rb/Sr ratio (>4.2 versus <2.5) and lower Ba content. These indicate that the precursor magma for Group 1 might be produced under vapour phase-absent conditions and that of Group 2 was possibly formed by H_2O-fluxing (Inger and Harris, 1993; Harris et al., 1995; Koester et al., 2002; Zhang et al., 2004a,b). Under fluid-absent conditions, muscovite starts to breakdown at ~700 °C, and biotite progressively breakdowns at ~850 °C (~5 kbar; Le Breton and Thompson, 1988; Tompson, 1996; Patiño-Dounce and Harris, 1998; Vielzeuf and Schmidt, 2001). Epidote/zoisite will melt and disappear at ~750–800 °C at ~10 kbar, 150–200 °C lower than that of amphibole (~920 °C; Lambert

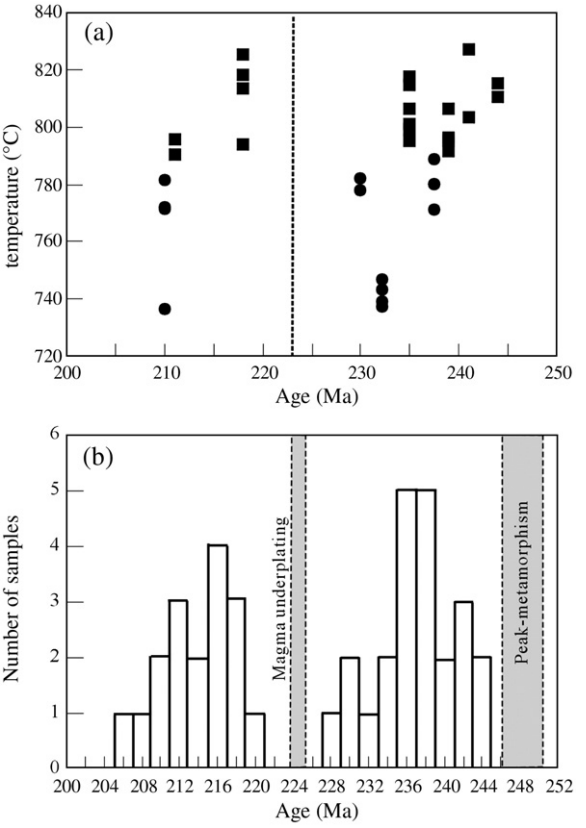

Fig. 11. (a) The diagram of temperature and age for the Indosinian granites in Hunan Province and (b) frequency of ages for the Indosinian granites in the SCB, respectively. Data in (b) are from Tables 3 and 4 and the following references (Wu et al., 1986; Shen et al., 1991; Li, 1994; Faure et al., 1996; Ge, 2003; Wang et al., 2003c; Wang, 2003; Xu et al., 2003; Deng et al., 2004; Qiu et al., 2004; Xie et al., 2004; Zhang et al., 2004a,b; Ding et al., 2005; Ma et al., 2005; Sun et al., 2005; Peng et al., 2006, in press). The age-data of peak metamorphism are from Chen et al. (1998) and Peng et al. (2004), and those of magma underplating is from Guo et al. (1997) and authors' unpublished data.

and Wyllie, 1972; Patiño-Dounce et al., 1990; Vielzeuf and Schmidt, 2001). Additionally, melting of Al-poor rocks in the presence of quartz and feldspar could generate metaluminous, Na- and Sr-rich melts, and peraluminous and K-rich melt commonly originated from an Al-rich source at 0.1–1.0 Gpa (Zen, 1986; Patiño-Dounce et al., 1990; Miller, 1995). Thus, taking into account the above-mentioned estimates of melting conditions, it is likely that mica-rich metapelititic source is predominantly dehydrated by the breakdown of muscovite, and the dehydration of metabasaltic source can be attributed to the breakdown of epidote/zoisite.

7. Geothermal constraints

Recent studies show that a tectonically convergent regime characterized by the thrusting/stack was predominantly developed in the SCB during Indosinian, especially early Indosinian (Peng et al., 1995; Chen, 1999; Wang et al., 2005b and authors' unpublished data). The early Indosinian mafic rocks associated with these intrusions are rarely observed in the SCB. However, when plotting the estimated temperatures versus the crystallization ages of all analyzed samples (Fig. 11a), the temperatures decrease with decrease of crystallization age during early Indosinian (243–228 Ma), suddenly increase at ~225 Ma, and subsequently decrease during late Indosinian (220–206 Ma). Additionally, a small amount of newly mantle-derived mafic magma with high $\varepsilon_{Nd}(t)$ values and low $^{87}Sr/^{86}Sr$ ratios (224–204 Ma; Guo et al., 1997) has been observed at Daoxian in southern Hunan Province, an indicative of a small-scale magma underplating event during late Indosinian in the region. These seem to suggest an important change of the heat supply at ~225 Ma in the region in spite of insignificant modification of magma sources.

7.1. Thermal-mechanical model

In attempt to better constrain the thermal-stress mechanism (tectonically crustal thickening versus magma underplating) for producing the Indosinian granites in the region, a FLAC (Fast Lagrangian Analysis of Continua) numerical simulation is presented.

Temperature evolution can be calculated from heat-diffusion equation (Ranalli, 1987)

$$\rho_{(Z,T)} C_{(T)} \partial T / \partial t = K_{(T)} \nabla^2 T + H$$

where $K_{(T)}$ is heat diffusivity, $\rho_{(Z,T)}$ is density, $C_{(T)}$ is specific heat capacity at constant pressure and H is heat productivity per unit of mass.

The mechanical behavior follows the elastic-plastic constitutive law (Jaeger and Cook, 1979)

$$\Delta\varepsilon = \Delta\varepsilon^e + \Delta\varepsilon^p,$$

where $\Delta\varepsilon^e$ is the elastic strain-increasing of the rocks before the plastic component is yielded and $\Delta\varepsilon^p$ is the plastic strain-increasing of the rocks after the plastic component is yielded.

7.2. Initial geological model and thermal and mechanical parameters

As introduced in geology setting presented above, the Proterozoic subduction/collision (~1.0 Ga) amalgamated the Yangtze and Cathaysian Blocks, and a Paleozoic intracontinental transtensional basin was followed (Li et al., 2002; Wang and Li, 2003). The basin geographically correspond to the distribution Indosinian granites (Fig. 1a), and is regard as a failed rift where the deep-sea turbidites with >12–15 km thickness were deposited. In contrast, only shallow-sea

Table 5
Material properties in thermal-mechanical simulated model

Lithology	TH			De	Co	Te	SM	BM	FA	DA	HC	HP
	YZ	FR	CA									
Layer 1 (sandstone+carbonate)	5	15	5	2400	5.0	1.5	1.04	1.39	10	2	2000	2.0
Layer 2 (slate+schist+gneiss)	20	9	20	2700	11.0	2.0	1.40	1.95	15	2	1200	3.6
Layer 3 (amphibolites+granulate)	10	11	10	2900	15.0	2.5	3.60	4.30	15	2	700	2.0

Note: TH: thickness; YZ: Yangtze Block; FR: failed rift; CA: Cathaysian Block; De: density, (kg m^{-3}); Co: cohesion, 10^6(Pa); Te: tension, 10^6(Pa); SM: shear modual, 10^{10}(Pa); BM: bulk modual, 10^{10}(Pa); FA: friction angle; DA: Dilation angle; HC: heat capacity, J/kg* K; HP: heat productivity. Layer 1, 2 and 3 are proposed on the basis of the geochemical data of their xenoliths and geophysical traverse in Hunan Province (Yuan et al., 1989; Qin, 1991; Guo et al., 1997; Lin et al., 1998; Wang et al., 2002). Layer 1 is represented by the Paleozoic sediment composed of the sandstone-slate and carbonate rock (15 km in the failed rift and 5 km on the outsides). Layer 2 is the folded basement of the Proterozoic gneiss and slate (10 km thick in the failed rift and 20 km thick on the sides). The crystallized basement is defined as Layer 3, which consists of amphibolite–granulites. The related material properties are from Jaeger and Cook (1979); Carter and Anderson (1982) and Wollenberg and Smith (1984).

carbonate rocks with 3–5 km thickness were deposited at its outsides (the interior of the Yangtze and Cathaysian blocks). Based on these geological observations in the region (e.g., Yuan et al., 1989; Qin, 1991; Guo et al., 1997; Lin et al., 1998; Wang et al., 2002), a geological model is constructed. In this model, the weak zone, equivalent to the Paleozoic failed rift, was considered. The zone is bounded between the surrounding stronger Yangtze and Cathaysian blocks. Layers 1, 2 and 3 in the model are characterized by the sandstone/slate/carbonate, schist/gneiss/slate and amphibolite/granulate, roughly corresponding to the Paleozoic sediments folded basement and crystallized basement, respectively (Yuan et al., 1989; Qin, 1991; Guo et al., 1997; Lin et al., 1998; Wang et al., 2002). The following initial conditions were adopted: crustal thickness of 35 km and lithospheric thickness of 80 km, temperature $T(0,0)=30$ °C at the surface. $\partial T/\partial z(z,0)=24$ °C/km at $0\ \text{km}<z\leq 35$ km and 10 °C/km at $35\ \text{km}<z\leq 80$ km. The specification of the model and their material parameters of the different rock-types (Jaeger and Cook, 1979; Carter and Anderson, 1982; Wollenberg and Smith, 1984; Wang et al., 2002) are listed in Table 5. The initial geometrical model, thermal equilibrium state prior to stress load and mechanical computation are shown in Fig. 12a.

7.3. Simulated result

7.3.1. Tectonical thickening of the continental crust

The simulated results show that temperature pattern was significantly modified in the weak zone but slightly on its outsides when the continental crust is progressively thickened from 35 km to ~47 km in response to the continuous shortening (Fig. 12b). In the weak zone, the temperature near to the base of the middle crust is up to that of muscovite dehydrated melting only when the initial crust (35 km) is tectonically thickened up to ~39 km (Wang et al., 2002). Under such a mechanically controlled melting condition, deformation strongly influences the mechanics of melt segregation at the source and is accommodated by melt-assisted granular flow (e.g., Rushmer, 2001; Vanderhaeghe and Teyssier, 2001). Muscovite-dehydrated melting results into positive volume change at the onset of melting, and produce enough internal dilatational strain, which further cracks the source rock to form an interconnected permeable melt network for promoting migration of the melt at <10 vol.% melting fractions (Rushmer, 2001; Vanderhaeghe and Teyssier, 2001; Rosenberg and Handy, 2005). When the continental crust is tectonically thickened to ~46 km even under the reaction-controlled melting condition, the temperature at the lower part of

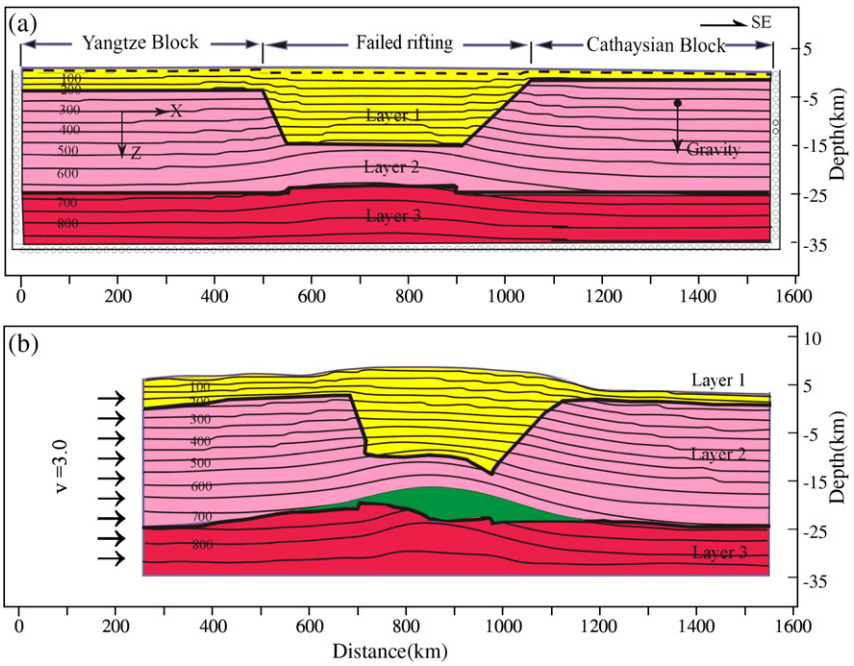

Fig. 12. (a) The initially geological model showing thermal equilibrium state before stress load and (b) the temperature pattern in the crust when the continental crust is tectonically thickened up to ~44 km from 35 km. The shade is the scale of the dehydration reaction of the mica-bearing source. The modeling parameters and detailed description is referred Table 5 and Wang et al. (2002).

Layer 2 as shown in Fig. 12b reaches to ~700–800 °C in the weak zone, resulting in the mica- and epidote/zoisite-dehydrated reaction to generate >20 vol.% melt fraction (Clemens and Vielzeuf, 1987). The simulated melting zone also coupled with the low-velocity seismic zone identified from the geophysical traverse in the region (e.g., Yuan et al., 1989; Chen, 1999). Thus such fractional melt might be effectively migrated upward to form magma chamber at the high level during the crustal shortening (e.g., Arzi, 1978; Clemens and Vielzeuf, 1987).

7.3.2. Underplating of mantle-derived magma

The simulated results indicate that the temperature of the country rocks rapidly increases and reach the maximum thermal perturbation by conductive heating within ~2 Ma just after underplating, assuming that a certain amount of mantle-derived magma (1000 °C) underplated into the crust under an initial thermal stable-state. Then the maximum thermal perturbation is gradually lessen to be a re-equilibrium of thermal state in the ~12 Ma afterward. The dehydration melting of the country rocks might be triggered by heat conduction to generate felsic magma prior to re-equilibrium of perturbed thermal state (<12 Ma), consistent with previous consideration (e.g., Koyaguchi and Kaneko, 1999). However, the scale of renascent magma is closely related to the volume of underplating magma. Similar conclusion can be referred to the pattern in Fig. 3 published by Wang et al. (2002).

8. Tectonic implications

The Indosinian granitic rocks are widespread not only in Hunan Province, but also in other regions in the SCB (Fig. 1). Our high-precisely geochronological data, together with recent zircon U–Pb ages from other areas in the SCB (Deng et al., 2004; Ding et al., 2005. Wu et al., 1986; Shen et al., 1991; Li, 1994; Faure et al., 1996; Ge, 2003; Wang et al., 2003c; Wang, 2003; Xu et al., 2003; Qiu et al., 2004; Xie et al., 2004; Xu et al., 2004; Zhang et al., 2004a,b; Ma et al., 2005; Sun et al., 2005; Peng et al., 2006, in press), indicate that these granites were mainly emplaced at ~243–206 Ma. The synthesis of these age-data is given in Background dataset 2. When all these data are statistically analyzed, they are clearly divided into two age-clusters: one is 243–228 Ma with a maximal frequency of ~236 Ma and the other is 220–206 Ma with maximal frequency of 218–214 Ma (Fig. 11b). Such results indicate that the peraluminous granites in the SCB were emplaced in two episodes, i.e. early and late Indosinian, not Hercynian and Indosinian as previously thought.

The geological observations show that the early Indosinian granites with an emplacement depth of 5–12 km extensively exposed to the surface. This indicates a denudation of the crustal materials with the thickness of >5–12 km since early Indosinian in the region. The current crustal thickness within the SCB is in the range of 35–40 km based on the available geophysical data (e.g., Yuan et al., 1989; Qin, 1991). In combination with the numerically modeling results, these data seem to support that the continental crust might be tectonically thickened up to ~47 km in the region during the early Indosinian period (Wang et al., 2002). Recent SHRIMP zircon U–Pb dating studies show that the metamorphic zircons, which occurred as single grains or overgrowth rims around older zircons in the high-grade metamorphic rocks in the SCB, gave the $^{207}Pb/^{206}Pb$ ages of 246–252 Ma (Chen et al., 1998; Peng et al., 2004). For example, the metamorphic zircons from granulite xenoliths hosted by charnokite intrusion in the Shiwan Mountains (southeastern Guangxi) yielded a weighted mean $^{207}Pb/^{206}Pb$ age of 248±6 Ma (Peng et al., 2004). Thus the metamorphic age of ~248 Ma might represent the time when the continental crust was tectonically thickened to a maximum. Just after the peak metamorphism, the over-thickened crust might have been isostatically re-adjusted, and the stress release at the shallow crust might be initiated. This is also evidenced by the following observations that; (1) the middle Triassic sequence is poorly exposed within the SCB; (2) the Paleozoic and lower Triassic strata experienced strong deformation characterized by thrust/stack, and uncomfortably underlay the upper Triassic clastics (HNGBMR, 1988; Peng et al., 1995; Chen, 1999; Wang et al., 2005b and references therein). During the readjusting of the over-thickened crust, the thermally mature zones of thickened crust was partially melted and then resulted into the generation of low-viscosity layer that may affect mechanical decoupling within the orogenic belt (Nelson et al., 1996; Schilling et al., 1997; Vanderhaeghe and Teyssier, 2001). The thermally weaken layer additionally led to the gravity-derived flow and thinning of the thickened crust and further promoted the partial melting of the source rocks (Vanderhaeghe and Teyssier, 2001). As a result, voluminous granitic magmas were formed and then segregated to at high levels (Le Fort et al., 1987; Singh et al., 2002). Such a process for the early Indosinian magma, involving in-situ radiogenic heating during collision and subsequent dehydrated reaction of the magma sources, is similar to that of the Himalayas–South Tibet, Central Andes and

North American Cordillera Orogen where the partial molten layer within the thickened continental crust is introduced, (e.g., Nelson et al., 1996; Schilling et al., 1997; Sylvester, 1998).

As shown in Fig. 11a, magma temperatures generally decrease with lowering of age between 243 Ma and 228 Ma. These indicate that in-situ radiogenic heating from the tectonically thickened crust might not be enough to further result in the production of the peraluminous felsic magma after ~228 Ma unless a new shortening event is accompanied or newly mantle-derived magma underplated into the crust. However, the late Indosinian transpressive/transextensive structures in the SCB, interpreted as the post-collisional signatures (e.g., Wang et al., 2005b), argue against the development of another stacking event. An alterative interpretation for the sudden increase of temperature at ~225 Ma and subsequent magma activity (220–206 Ma), as shown in Fig. 11a–b, is a likely result of the magma underplating event. This possibility is supported by the occurrence of gabbroic xenoliths (with the formation age of 224 Ma) hosted in Cretaceous Daoxian basalt, which is interpreted as the earliest underplating magma during the Indosinian period in the SCB (Guo et al., 1997). It is common that the compressive stress might have been released at ~5–20 Ma after the peak stacking of the crust (e.g., Patiño-Dounce et al., 1990). The stress discharge might benefit for the underplating of newly small-volume new magma in response to the lithospheric delamination or upwelling of asthenosphere. In combination with the above-mentioned consideration that the peraluminously Indosinian granites originated from either the metapelitic-dominated source (Group 1) or mixing of metapelitic and metabasaltic sources (Group 2), it is inferred that the newly mantle-derived magma was insufficient to rise to the melting depths for generating the granitic rocks, and to mix with the crust-derived melt. Thus it is most likely that heat energy from the newly underplating magma was transferred to the melting source by conduction. Our numerical modeling results support such a consideration.

A series of studies showed that the lithospheric extension in the SCB was predominately developed after ~175 Ma (e.g., Wang et al., 2003a,b, 2005c) and the early Indosinian structures were dominated by stacking/shortening in the SCB (e.g., Chen, 1999; Wang et al., 2005b). Thus the Indosinian peraluminous granites in the SCB were most likely the product of the collision-related magmatism. Two possibilities involving the oceanic/arc-continental collision and intracontinental collision can be put forward. However, early Mesozoic ophiolite suites, oceanic basins and arc magmatism were not observed in the SCB. This, together with the planar-shaped distribution of these granites (e.g., Wang et al., 2005a), argues against the occurrence of Indosinian oceanic/arc-continental subduction/collision in the SCB. The westward subduction of a Pacific plate identified by the paleomagnetic data might not be initiated until ~125 Ma (Engebretson et al., 1985). Thus, the Indosinian peraluminous granites in the SCB might be the result of intracontinental collision involving the failed rift (acted as a weak zone) bounded by the Yangtze and Cathaysian basements (acted as the strong vise), as evidenced by the structural observations in the SCB (e.g., Wang et al., 2005b). The variations in sedimentary thickness in the failed rift and its heterogeneous thermal state may have important impact on localizing intracontinental deformation, as case in central Australia (Sandiford and Hand, 1998, 2001). Question remains as to what is the external dynamic mechanism for causing the early Indosinian intracontinental compression in the SCB?

Contemporaneous with the tectonically crustal thickening in the SCB, there occurs subduction/collision around the SCB, although maybe not along the eastern margin. At the northern margin, the Yangtze block subducted toward the north during early Triassic and subsequently collided with the North China Block along the Dabie–Sulu Orogeny (e.g., Li et al., 1993; Hacker et al., 1998). At the southwestern margin, the closure of the paleo-Tethys ocean and continent–continent collision occurred between early Permian and middle Triassic, and the postcollisional collapse developed during late Triassic (e.g., Cong et al., 1993; Zhong, 1998; Peng et al., 2006, in press). The collision of the Northern Indosinian block with the SCB was dated at 258–242 Ma along the Song-Ma belt (e.g., Carter et al., 2001; Lepvrier et al., 2004). Such a coupling suggests a close relationship between the orogens around the SCB and intracontinental collision in the SCB during early Indosinian. Here we propose that the early Indosinian subduction/collision at southwestern margin of the SCB, coupling with above-mentioned special tectonic nature within the SCB, resulted in the contemporaneously intracontinental collision in the SCB, accompanied by the continental crustal thickening and early-Indosinian granitic magmatism when the North China and Northern Indosinian blocks acted as the restricted boundary, and the Pacific Plate as an unlimited boundary. The underplating of small amount of magma during the postcollisional collapse provides enough heat energy through heat conduction and induced the dehydrated melting of the country rocks to generate late-Indosinian peraluminous granites.

Acknowledgements

We are grateful to Prof. S Foley and two anonymous reviewers for their critical and constructive review, which led to major improvement of the manuscript. This study was financially supported by the National Nature Sciences Foundation of China (40334039, 40421303, 40473019), Hong Kong RGC Project (HKU7041/05P), China Petroleum and Chemical Corporation and Chinese Academy of Sciences.

Appendix A. Supplementary data

Supplementary data associated with this article can be found, in the online version, at doi:10.1016/j.lithos.2006.11.010.

References

Altherr, R., Holl, A., Hegner, E., Langer, C., Kreuzer, H., 2000. High-potassium, calc-alkaline plutonism in the European Variscides: northern Vosges (France) and northern Schwarzwald (Germany). Lithos 50, 51–73.

Anthony, E.Y., 2005. Source regions of granites and their links to tectonic environment: examples from the western United States. Lithos 80, 61–74.

Arzi, A.A., 1978. Critical phenomena in the rheology of partially melted rocks. Tectonophysics 44, 173–184.

Carter, N.L., Anderson, D.A., 1982. Creep and creep rupture of granitic rocks. Am. Geophys. Union, Geophys. Monogr. 24, 61–82.

Carter, A., Roques, D., Bristow, C., 2001. Understanding Mesozoic accretion in southeast Asia: significance of Triassic thermotectonism (Indosinian orogen) in Vietnam. Geology 29 (3), 211–214.

Chappell, B.W., White, A.J.R., 1992. I- and S-type granites in the Lachlan fold belt. Trans. R. Soc. Edinb. Earth Sci. 83, 1–26.

Chen, A., 1999. Mirror-image thrusting in the South China orogenic belt: tectonic evidence from western Fujian, southeastern China. Tectonophysics 305, 497–513.

Chen, J.F., Jahn, B.M., 1998. Crustal evolution of southeastern China: Nd and Sr isotopic evidence. Tectonophysics 284, 101–133.

Chen, D.F., Li, X.H., Pang, J.M., Dong, W.Q., Chen, G.Q., Chen, X.P., 1998. Metamorphic newly producted zircon, SHRIMP ion microprobe U–Pb age of amphibolite of Hexi Group, Zhejiang and its implication. Acta. Mineral. Sin. 18 (4), 396–400.

Clemens, J.D., Vielzeuf, D., 1987. Constraints on melting and magma production in the crust. Earth Planet. Sci. Lett. 86, 287–306.

Compston, W., Williams, I.S., Kirschvink, J.L., Zhang, Z., Ma, G., 1992. Zircon U–Pb ages for the Early Cambrian time-scale. Geol. Soc. (Lond.) 149, 171–184.

Cong, B.L., Wu, G.Y., Zhang, Q., Zhang, R.Y., Zhai, M.G., Zhao, D.S., Zhang, W.H., 1993. Petrotectonic evolution of the Tethys zone in western Yunnan, China. Chin. Bull. (B) 23 (11), 1201–1207 (in Chinese).

Deng, X.G., Chen, Z.G, Li, X.H., 2004. SHRIMP U–Pb zircon dating of the Darongshan–Shiwandashan. Geol. Rev. 50 (4), 426–432.

Deprat, J., 1914. Etude des plissements et des zones décrasement de la moyenne et de la basse Rivière Noire. Mem. Serv. Geol. Indoch. 3, 59.

Ding, X., Chen, P.R., Chen, W.F., Huang, H.Y., Zhou, X.M., 2005. LA-ICPMS zircon dating of Weishan granitic plutons in Hunan Province: petrogenesis and tectonic implications. Sci. China (D) 35 (7), 606–616.

Dostal, J., Chatterjee, A.K., 2000. Contrasting behaviour of NbrTa and ZrrHf ratios in a peraluminous granitic pluton_Nova Scotia, Canada. Chem. Geol. 163, 207–218.

Ellis, D.J., Thompson, A.B., 1986. Subsolidus and partial melting reactions in the quartz-excess $CaO+MgO+Al_2O_3+SiO_2+H_2O$ system under water-excess and water-deficient condients to 10kb: some implications for the origin of peraluminous melts from mafic rocks. J. Petrol. 27, 91–121.

Engebretson, D.C., Cox, A., Gordon, R.G., 1985. Relative motions between oceanic and continental plates in the Pacific basins. Geol. Soc. Am., Spec. Pap. 206, 1–59.

Faure, M., Sun, Y., Shu, L., Monié, P., Charvet, J., 1996. Extensional tectonics within a subduction-type orogen: the case study of the Wugongshan dome (Jiangxi Province, southeastern China). Tectonophysics 263, 77–106.

Fromagat, J., 1932. Sur la structure des Indosinides. C. R. Acad. Sci. 195, 538.

Gao, S., Lin, W.L., Qiu, Y.M., 1999. Contrasting geochemical and Sm–Nd isotopic compositions of Archaean metasediments from the Kongling high-grade terrain of the Yangtze craton: evidence for cratonic evolution and redistribution of REE during crustal anatexis. Geochim. Cosmochi. Acta 13/14, 2071–2088.

Gaudemer, Y., Jaupart, C., Tapponnier, P., 1988. Thermal control on postorogenic extension in collision belts. Earth Planet. Sci. Lett. 89 (1), 48–62.

Ge, X.Y., 2003. Mesozoic magmatism in Hainan island (SE China) and its tectonic implications: geochronology, geochemical and Sr–Nd isotope evidences, PhD thesis, Guangzhou Institute of Geochemistry, Chinese Academy of Sciences 1–83.

Guo, F., Fan, W.M., Lin, G., Lin, Y.X., 1997. Sm–Nd dating and petrogenesis of Mesozoic gabbro xenolith in Daoxian County, Hunan Province. Chin. Sci. Bull. 42, 1661–1663.

Hacker, B.R., Ratschbacher, L.W., Ireland, L., 1998. U/Pb zircon ages constrain the architecture of the ultrahigh-pressure Qinling–Dabie Orogen, China. Earth Planet. Sci. Lett. 161, 215–230.

Harris, N., Ayres, M., Massey, J., 1995. Geochemistry of granitic melts produced during the incongruent melting of muscovite-implications for the extraction of Himalayan leucogranite magmas. J. Geophys. Res. 100, 15767–15777.

Healy, B., Collins, W.J., Richards, S.W., 2004. A hybrid origin for Lachlan S-type granites: the Murrumbridgee batholith example. Lithos 79, 197–216.

HNGBMR (Bureau of Geology and Mineral Resources of Hunan Province), 1988. Regional Geology of the Hunan Province. Geological Publishing House, Beijing, pp. 286–507 (in Chinese with English summary).

Huang, J.Q., Ren, J.S., Jiang, C.F., Zhang, Z.K., Qin, D.Y., 1987. Geotectonic Evolution of China. Springer-Verlag, Berlin. 1–203 pp.

Inger, S., Harris, N.B.W., 1993. Geochemical constraints on leucogranite magmatism in the Langtang Valley, Nepal Himalaya. J. Petrol. 34, 345–368.

Jackson, S.E., Pearson, N.J., Griffin, W.L., Belousova, W.A., 2004. The application of laser ablation-inductively coupled plasma-mass spectrometry to in situ U–Pb zircon geochronology. Chem. Geol. 211 (1–2), 47–69.

Jaeger, J.C., Cook, N.G.W., 1979. Fundamentals of Rock Mechanics. Chapman and Hall, London, pp. 1–593.

Johannes, W., Holtz, F., 1996. Petrogenesis and Experimental Petrology of Granitic Rocks. Springer, Berlin. 1–335 pp.

Jung, S., Hoernes, S., Mezger, K., 2000. Geochronology and petrogenesis of Pan-African, syn-tectonic, S-type and post-tectonic A-type granite (Namibia): products of melting of crustal sources, fractional crystallization and wall rock entrainment. Lithos 50, 259–287.

Jung, S., Mezger, K., Hoernes, S., 2003. Petrology of basement-dominated terranes II. Contrasting isotopic (Sr, Nd, Pb and O) signatures of basement-derived granites and constraints on the source region of granite (Damara orogen, Namibia). Chem. Geol. 199, 1–28.

JXGBMR (Bureau of Geology and Mineral Resources of Jiangxi Province), 1984. Regional Geology of the Jiangxi Province. Geological Publishing House, Beijing, pp. 1–921 (in Chinese with English summary).

Kalsbeek, F., Jepsen, H.F., Nutman, A.P., 2001. From source migmatites to plutons: tracking the origin of ca. 435 Ma S-type granites in the East Greenland Caledonian Orogen. Lithos 57, 1–21.

Koester, E., Pawley, A.R., Luĩ, A.D., Fernandes, L.A.D., Porcher, C.C., Soliani Jr., E., 2002. Experimental melting of cordierite gneiss and the petrogenesis of syntranscurrent peraluminous granites in Southern Brazil. J. Petrol. 43, 1595–1616.

Koyaguchi, T., Kaneko, K., 1999. A two-stage thermal evolution model of magmas in continental crust. J. Petrol. 40 (2), 241–254.

Lambert, I.B., Wyllie, P.J., 1972. Melting of gabbro (quartz eclogite) with excess water to 35 kb, with geological applications. J. Geol. 80 (6), 693–708.

Le Breton, N., Thompson, A.B., 1988. Fluid-absent (dehydration) melting of biotite in metapelites in the early stages of crustal crustal anatexis. Contrib. Mineral. Petrol. 99, 226–237.

Le Fort, P., Cuney, M., Denniel, C., France-Lanord, C., Sheppard, S.M.F., Upreti, B.N., Vidal, P., 1987. Crustal generation of the Himalayan leucogranites. Tectonophysics 134, 39–57.

Lepvrier, C., Maluski, H., Tich Vu, Van, Leyerloup, A., Phan Truong, T., Nguyen Van, V., 2004. The Early Triassic Indosinian orogeny in Vietnam (Truong Son Belt and Kontum Massif); implications for the geodynamic evolution of Indochina. Tectonophysics 393, 87–118.

Li, X.H., 1994. A compressive U–Pb, Sm–Nd, Rb–Sr and ^{40}Ar–^{39}Ar geochronological study on Guidong granodiorite, southeast China: Records of multiple tectonothermal events in a single pluton. Chem. Geol. 115, 283–295.

Li, S.G., Chen, Y., Cong, B.L., Zhang, Z., Zhang, Y., Liou, D.L., Hart, S.A., Ge, N., 1993. Collision of the North China and Yangtze Blocks and formation of coesite-bearing eclogites: timing and processes. Chem. Geol. 109, 80–89.

Li, Z.X., Li, X.H., Zhou, H.W., Kinny, P.D., 2002. Grenvillian continental collision in south China: new SHRIMP U–Pb zircon results and implications for the configuration of Rodinia. Geology 2, 163–166.

Liang, X.R., Wei, G.J., Li, X.H., Liu, Y., 2003. Precise measurement of $^{143}Nd/^{144}Nd$ and Sm/Nd ratios using multiple-collectors inductively couple plasma-mass spectrometer (MC-ICP-MS). Geochimica 32 (1), 91–96.

Lin, G., Fan, W.M., Guo, F., 1998. The crust-mantle transitional zone and its tectonic evolution. Geotecton. Metallogen. 11–18 (Supp).

Ludwig, K.R., 2001. Sqiud 1.02: a user manual. Berkeley Geochronological Center Special Publiccation, pp. 1–219.

Ma, T.Q., Bai, d.Y., Kuang, J., Wang, X.H., 2005. Zircon SHRIMP dating of the Xietian granite pluton, Chaling, Southeastern hunan and its geological significance. Geol. Bull. China 24 (5), 415–419.

Miller, C.F., 1995. Are strongly peraluminous magmas derived from pelitic sedimentary sources? J. Geol. 93, 673–689.

Nelson, K.D., et al., 1996. Partially molten middle crust beneath southern Tibet: synthesis of project INDEPTH results. Science 274 (5293), 1684–1688.

Patiño-Dounce, A.E., Harris, N., 1998. Experimental constraints on Himalayan anatexis. J. Petrol. 39, 689–710.

Patiño-Dounce, A.E., Humphreys, E.D., Johnston, A.D., 1990. Anatexis and metamorphism in tectonically thickened continental crust exemplified by the Sevier hinterland, western North America. Earth Planet. Sci. Lett. 97, 290–315.

Peng, S.M., Fu, L.F., Zhou, G.Q., 1995. Tectonic evolution of Yunkai massif and its shearing anatectic origin of gneissicgranitic rocks. China Univ. Geosciences Press, Wuhan, pp. 1–165.

Peng, S.B., Fu, J.Y., Lou, Y.H., 2004. The discovery and significance of A-type charnokite in southeast Guangxi Province, China. Sci. Technol. Eng. 4 (10), 832–834.

Peng, B.X., Wang, Y.J., Fan, W.M., Peng, T.P., Liang, X.Q., in press. LA-ICPMS zircon U–Pb dating for three typical granitic plutons from Central Hunan and western Guangdong Provinces and its petrogenetic implications. Acata Geologica Sinica.

Peng, T.P., Wang, Y.J., Fan, W.M., Liu, D.Y., Shi, Y.R., Miao, L.C., 2006. The SHRIMP zircon U–Pb geochronology of the early Mesozoic felsic igneous rocks from the southern Lancangjiang and its tectonic implications. Sci. in China (series D). 49 (10), 1032–1042.

Qi, L., Hu, J., Greggoire, C., 2000. Determination of trace elements in granites by inductively coupled plasma mass spectrometry. Talanta 51, 507–513.

Qin, B.H., 1991. Deep-seated structure beneath Hunan Province revealed by Taiwang–Heishui geotravers. Hunan Geol. 15, 89–96 (in Chinese with English abstract).

Qiu, Y.M., Gao, S., McNaughton, N.J., Groves, D.I., Ling, W.L., 2000. First evidence of >3.2 Ga continental crust in the Yangtze craton of South China and its implications for Archean crustal evolution and phanerozoic tectonics. Geology 28 (1), 11–14.

Qiu, J.S., McInnes, B.I.A., Xu, X.S., Allen, C.M., 2004. Zircon ELA-ICPMS dating for Wuliting pluton at Dajishan, southern Jiangxi and new recognition about its relationship to Tungsten mineralization. Geol. Rev. 50 (2), 125–133.

Ranalli, G., 1987. Rheology of the Earth. Allen and Unwin, London, pp. 1–366.

Ren, J.S., 1991. On the geotectonics of southern China. Acta Geol. Sin. 2, 111–136.

Rosenberg, C.L., Handy, M.R., 2005. Experimental deformation of partially melted granite revisited: implications for the continental crust. J. Metamorph. Geol. 23, 19–28.

Rushmer, T., 2001. Volume change during partial melting reactions: implications for melt extraction, melt geochemistry and crustal rheology. Tectonophysics 342, 389–405.

Sandiford, M., Hand, M., 1998. Control on the locas of intraplate defoemation in central Australia. Earth Planet. Sci. Lett. 162, 97–110.

Sandiford, M., Hand, M., 2001. Tectonic feedback, intraplate orogeny and the geochemical structure of the crust: a central Australian perspective. In: Miller, J.A., Holdsworth, R.E., Buick, I.S., Hand, M. (Eds.), Continental Reactivation and Reworking. Geol. Soc. London, Spec. Pub., vol. 184, pp. 195–218.

Schilling, F.R., Partzsch, G.M., Brasse, H., Schwarz, G., 1997. Partial melting below the magmatic arc in the central Andes deduced from geoelectromagnetic field experiments and laboratory data. Phys. Earth Planet. Inter. 103, 17–31.

Shen, J., Zhao, Y.Y., Liu, D.Z., 1991. Study on Sr–O–Pb and S isotopes of granitic body in Zhuguangshan, South China. Acta Pet. Sin. 2, 38–42 (in Chinese).

Shen, W.Z., Ling, H.F., Li, W.X., Wang, D.Z., 1998. Sr and Nd isotope of Mesozoic granitoids in Jiangxi Province. Chin. Sci. Bull. 43, 2653–2657.

Singh, S., Mukherjee, P.K., Jain, A.K., Khanna, P.P., Saini, N.K., Kumar, R., 2002. Source characterization and possible emplacement mechanism of collision-related Gangotri leucogranite along Bhagirathi Valley, NW-Himalaya. J. Virtual Explor. 11, 15–26.

Stein, H.J., Crook, J.G., 1990. Late Cretaceous–Tertiary magmatism in the Colorada Mineral Belt: rare earth element and Sr–Nd isotopic studies. Mem. Geol. Soc. Amer. 174, 195–224.

Sun, S.S., McDonough, W.F., 1989. Chemical and isotopic systematics of oceanic basalts: implication for mantle composition and processes. In: Saunder, A.D., Norry, M.J. (Eds.), Magmatism in the ocean basins. Geol. Soc. Spec. Publ., vol. 42, pp. 313–345.

Sun, T., Zhou, X.M., Chen, P.R., Li, H.M., Zhou, H.Y., Wang, Z.C., Shen, W.Z., 2005. Strongly peraluminous granites of Mesozoic in Eastern Nanling Range, southern China: petrogenesis and implications for tectonics. Sci. China (Series D) 48 (2), 165–174.

Sylvester, P.J., 1998. Postcollisional strongly peraluminous granites. Lithos 45, 29–44.

Taylor, S.R., McLennan, S.M., 1985. The continental crust: Its composition and evolution. Oxford Press Blackwell, pp. 1–312.

Tompson, A.B., 1996. Fertility of crustal rocks during anatexis. Trans. R. Soc. Edinb. Earth Sci. 87, 1–10.

Vanderhaeghe, O., Teyssier, C., 2001. Partial melting and flow of orogens. Tectonophysics 342, 451–472.

Vielzeuf, D., Schmidt, N.W., 2001. Melting relations in hydrous systems revisited: application to metapelites, metagreywackes and metabasalts. Contrib. Mineral. Petrol. 141, 251–267.

Wu, G.Y., Zhang, Y.Z., Hoehndofr, A., 1986. Geochronology of Guangning granitic complex. Geol. Guangdong 1 (1), 1–22 (in Chinese).

Wang, Z.C., 2003. Crust-derived magmatism and uranium mineralization in Hunan-Guangxi Provinces, Nanling areas. PhD thesis, Nanjing Univ. 1–70.

Wang, J., Li, Z.X., 2003. History of Neoproterozoic rift basins in South China: implications for Rodinia break-up. Precambrian Res. 1–4, 141–158.

Wang, Y.J., Zhang, Y.H., Fan, W.M., Xi, X.W., Guo, F., Lin, G., 2002. Numerical modeling for generation of Indosinian peraluminous granitoids Hunan Province: basaltic underplating versus tectonic thickening. Sci. China (D series) 45 (11), 1042–1056.

Wang, Y.J., Fan, W.M., Guo, F., 2003a. Geochemistry of early Mesozoic K-rich dioritic–granodioritic intrusions in Southeastern Hunan Province, South China: petrogenesis and tectonic implications. Geochem. J. 37 (4), 427–448.

Wang, Y.J., Fan, W.M., Guo, F., Peng, T.P., Li, C.W., 2003b. Geochemistry of Mesozoic mafic rocks around the Chenzhou–Linwu fault in South China: implication for the lithospheric boundary between the Yangtze and the Cathaysia Blocks. Int. Geol. Rev. 45 (3), 263–286.

Wang, Q., Zhao, Z.H., Jian, P., 2003c. SHRIMP U2Pb zircon geochronology of Yangfang aegiriteaugite syenite in Wuyi Mountains of South China and its tectonic implications. Chin. Sci. Bull. 48 (20), 2241–2247.

Wang, Y.J., Fan, W.M., Liang, X.Q., Peng, T.P., Shi, Y.R., 2005a. SHRIMP zircon U–Pb geochronology of Indosinian granites in Hunan Province and its petrogenetic implications. Chin. Sci. Bull. 50 (13), 1395–1403.

Wang, Y.J., Zhang, Y.H., Fan, W.M., Peng, T.P., 2005b. Structural signatures and $^{40}Ar/^{39}Ar$ geochronology of the Indosinian Xuefengshan transpressive belt, South China Interior. J. Struct. Geol. 27, 985–998.

Wang, Y.J., Fan, W.M., Peng, T.P., Guo, F., 2005c. Element and Sr–Nd systematics of early Mesozoic volcanic sequence in southern Jiangxi Province, South China: petrogenesis and tectonic implications. Int. J. Earth Sci. 53 (1), 53–65.

Watson, E.B., Harrison, T.M., 1983. Zircon saturation revisited: temperature and composition effects in a variety of crustal magma types. Earth Planet. Sci. Lett. 64, 295–304.

Williams, I.S., 1998. U–Th–Pb geochronology by ion microprobe. In: McKibben, M.A., Shanks III, W.C., Ridley, W.I. (Eds.), Applications of Microanalytical Techniques to Understanding Mineralizing Processes. Rev. in Economic Geol., vol. 7, pp. 1–35.

Wollenberg, H.A., Smith, A.P., 1984. Radiogenic heat production of crustal rocks: a compilation from unpublished data and the geochemical literature. Trans. Am. Geophys. Union 65, 1121.

Xie, C.F., Zhu, J.C., Ding, S.J., 2004. Hercynian–Indosinian mafic–ultramafic intrusion in Hainan Island, constrains on the lithospheric thinning during post-collisional phase. The Seminar Abstracts of 2004 National Petrology and Geodynamics, pp. 289–290 (in Chinese).

Xu, X.S., Deng, P., O'Reilly, S.Y., Griffin, W.L., Zhou, X.M., Tan, Z.Z., 2003. Single zircon LAM_ICPMS U–Pb dating of Guidong complex (SE China) and its petrogenetic significance. Chin. Sci. Bull. 48 (17), 1892–1899.

Xu, H.J., Ma, C.Q., Zhong, Y.F., Yu, Z.B., 2004. Zircon SHRIMP dating of granites from Taojiang and Dashenshan plutons in Hunan Province: constrains on the lower age of collision of Yangtze and Cathaysian Blocks. The Seminar Abstracts of 2004 National Petrology and Geodynamics, pp. 312–314 (in Chinese).

Yuan, H.L., Wu, F.Y., Gao, S., Liu, X.M., Xu, P., Sun, D.Y., 2003. LA-ICPMS Zircon U–Pb age and REE of Cenozoic pluton in NE China. Chin. Sci. Bull. 48 (14), 1511–1520.

Yuan, X.C., Zuo, Y.M., Cai, Y.L., Zhou, J.X., 1989. The structure of the lithosphere and the geophysics in South China Block. In: the editorial board of bulletin of Geophysic (eds) Progress on geophysics in China in the 1980s, Beijing, Science Press, 243–249.

Zen, E., 1986. Aluminum enrichment in silicate melts by fractional crystallization: some mineralogic and petrographic constrains. J. Petrol. 27, 1095–1117.

Zhang, H.F., Harris, N., Parrish, R., Kelley, S., Zhang, L., Rogers, N., Argles, T., King, J., 2004a. Causes and consequences of protracted melting of the mid-crust exposed in the North Himalayan antiform. Earth Planet. Sci. Lett. 228, 195–212.

Zhang, G.W., Hua, R.M., Wang, R.C., Li, H.M., Chen, P.R., 2004b. Single zircon U–Pb isotopic age of the Wuliting granite in Dajishan area of Jiangxi and its geological implication. Acta Geol. Sin. 78 (3), 352–358.

Zhong, D.L., 1998. Paleotethyan Orogenic Belts in Yunnan and Western Sichuan. Sci. Press, Beijing, pp. 1–230.